The Valanginian Weissert Event on the south Tethyan margin: a dynamic paleoceanographic evolution based on the study of calcareous nannofossils.

Majd Shmeit, F. Giraud, E. Jaillard, S. Reboulet, M. Masrour, J.E. Spangenberg, A. El-Samrani

The Valanginian Weissert Event on the south Tethyan margin: a dynamic paleoceanographic evolution based on the study of calcareous nannofossils

M. Shmeit[1,2*], F. Giraud[1], E. Jaillard[1], S. Reboulet[3], M. Masrour[4], J.E. Spangenberg[5], A. El-Samrani[2]

1. Univ. Grenoble Alpes, Univ. Savoie Mont Blanc, CNRS, IRD, Univ. Gustave Eiffel, ISTerre, 38000 Grenoble, France

2. Lebanese University, Doctoral School of Science and Technology, Laboratory of Geosciences Georesources and Environment L2GE, EDST/PRASE, Beirut, Lebanon

3. Univ Lyon, UCBL, ENSL, UJM, CNRS, LGL-TPE, F-69622, Villeurbanne, France

4. Université Ibn Zohr, Faculté des Sciences, Département de Géologie, BP 8106, Cité Dakhla, Agadir, Morocco

5. University of Lausanne, Institute of Earth Surface Dynamics (IDYST), CH-1015 Lausanne, Switzerland

* corresponding author: majd.homaidan-shmeit@u-bourgogne.fr

Highlights:

- Paleoceanographic reconstruction around the Weissert Event in the southern Tethys
- High surface-water fertility and nannofossil production during the Weissert Event
- Major impact of sea-level and river clastic input on the nannofossil community
- Sea level fall caused the nannoconid decline before the Weissert Event
- Nannoconid recovery was associated with high surface-water fertility

ABSTRACT:

Paleoceanographic conditions across the Valanginian Weissert oceanic anoxic event were reconstructed for the first time on the central Moroccan margin from a quantitative-based calcareous nannofossil study. Two onshore successions in the Essaouira-Agadir Basin and one offshore from DSDP Hole 416A were studied, providing a proximal-distal transect on the central Moroccan margin. The paleoceanographic conditions were reconstructed in an accurate chronostratigraphic framework. The sedimentary evolution of the Essaouira-Agadir Basin shows that sea-level variations controlled the paleogeographic context, clastic input, and nutrient availability. A thick photic zone and mesotrophic conditions favored the development of a diverse nannofossil community before the Weissert Event in the early Valanginian. In all studied successions, a collapse of the nannofossil community was recorded during the onset of the Weissert Event at the early-late Valanginian transition, and was caused by a major sea-level fall. The nannofossil community gradually recovered and reached its highest nannofossil production associated with high surface-water fertility during the Weissert Event in the late Valanginian. This eutrophication is coeval with the high and stable $\delta^{13}C_{carb}$ values of the carbon-isotope positive shift. After the Weissert Event, surface-water fertility and nannofossil production decreased but remained higher than during the early Valanginian. Additionally, the nannoconid decline started in the early Valanginian and was linked to a low sea-level. Their recovery in the early late Valanginian occurred during conditions of high sea-level and of high surface-water fertility. The central Moroccan margin is integrated into a global paleoceanographic reconstruction.

Keywords: Carbon isotope excursion; Central Moroccan margin; Biostratigraphy; Sedimentary evolution; Surface-water fertility

1. Introduction

The Valanginian stage (137.7 – 132.6 Ma; Gale et al., 2020) records the first positive carbon-isotope excursion (CIE) of the Early Cretaceous (Lini et al., 1992; Weissert and Erba, 2004), termed the Weissert oceanic anoxic event or the Weissert Event (Erba et al., 2004; Kujau et al., 2012). The amplitude of the CIE ranges between 1.5–2 ‰ in bulk marine carbonate rock and 1.5–3 ‰ in marine organic matter (Lini et al., 1992; Hennig et al., 1999; McArthur et al., 2007; Charbonnier et al., 2013). In addition, the positive CIE was recognized in terrestrial fossil plants with a magnitude of ~4 ‰, implying a perturbation of both the oceanic and atmospheric Earth systems (Gröcke et al., 2005; Nunn et al., 2010). Martinez et al. (2015) identified three phases for the CIE, a first phase of rapid $\delta^{13}C_{carb}$ increase with a duration of 0.60 myr, a second phase of stable $\delta^{13}C_{carb}$ values lasting 1.48 myr, and a final phase of smooth decrease in $\delta^{13}C_{carb}$ values lasting 3.77 myr and extending to the early-late Hauterivian boundary. The onset of the positive CIE was observed just below the early-late Valanginian boundary (Duchamp-Alphonse et al., 2007; McArthur et al., 2007; Gréselle et al., 2011; Martinez et al., 2015). In the Tethyan Realm, the positive CIE was dated from the late NK3A calcareous nannofossil Subzone and extends to the NC4A calcareous nannofossil Subzone in some localities (Lini et al., 1992; Sprovieri et al., 2006; Duchamp-Alphonse et al., 2007; Bornemann and Mutterlose, 2008; Charbonnier et al., 2013; Aguado et al., 2018). Calibrated with ammonite biostratigraphy, the onset of the positive CIE was identified in the lower part of the *Karakaschiceras inostranzewi* Standard Zone (uppermost early Valanginian) and the highest values occur during the *Saynoceras verrucosum* Standard Zone (lowermost late Valanginian; McArthur et al., 2007; Gréselle et al., 2011; Martinez et al., 2015; Aguado et al., 2018). The aforementioned zones follow the standard ammonite zonation that is suitable for the Mediterranean Province of the Mediterranean-Caucasian Subrealm (Tethyan Realm; Reboulet et al., 2018). In addition to the Tethyan Realm, records of the positive CIE extend to a wide range of geographic locations that

include the Atlantic Ocean (Brenneke, 1978; Cotillon and Rio, 1984), the northwestern Pacific Ocean (Bartolini, 2003), the Boreal Realm (Price and Mutterlose, 2004; Meissner et al., 2015; Morales et al., 2015), and the southern Hemisphere (Aguirre-Urreta et al., 2008; Gómez-Dacal et al., 2018).

The positive CIE has been associated with a global increase in marine surface-water primary productivity (Erba et al., 2004). During the Valanginian, calcareous nannofossils and dinoflagellates were the major marine planktonic primary producers (Bown et al., 2004). Several studies on calcareous nannofossil assemblages have shown enhanced surface-water trophic conditions occurring before and during the Weissert Event, inferred from increasing abundances of high-fertility taxa such as *Biscutum*, *Discorhabdus*, *Diazomatolithus*, and small *Zeugrhabdotus* spp. (Tethyan Realm: Bersezio et al., 2002; Erba and Tremolada, 2004; Duchamp-Alphonse et al., 2007; Mattioli et al., 2014; Atlantic Ocean: Bornemann and Mutterlose, 2008; Kessels et al., 2006; Pacific Ocean: Lozar and Tremolada, 2003; and Boreal Realm: Williams and Bralower, 1995; Melinte and Mutterlose, 2001; Kessels et al., 2006). Nevertheless, paleoceanographic reconstructions based on calcareous nannofossils from the south Tethyan margin have not been documented yet, such that it needs to be further investigated. The causes of the increase in marine primary productivity differ in coastal and distal pelagic settings. Eutrophication in the coastal settings is hypothesized to have been caused by a greenhouse climate, intensification of the hydrological cycle, and consequently higher weathering rates and detrital input (Lini et al., 1992). Climate reconstructions demonstrated intensified hydrolyzing conditions culminating around the early-late Valanginian transition observed from clay mineral distributions (Duchamp-Alphonse et al., 2011; Charbonnier et al., 2020) and spore-pollen ratios (Kujau et al., 2013). Eutrophication in pelagic settings could be explained by the introduction of limiting bio-metals from hydrothermal vents during the break-up of Gondwana (Lini et al., 1992; Weissert et al., 1998; Erba et al., 2004). Sea-level changes

might have also influenced the fertilization of the ocean. (1) Enhanced continental runoff increases nutrient fluxes to the proximal parts of the ocean (gradual fertilization) during low sea level. (2) An increase in nutrients within the outer shelf realm may be linked to upwelling (sharp fertilization) during high sea level. In the late Valanginian, a global sea-level rise was documented after an all-time minimum of the Early Cretaceous occurred in the mid-Valanginian (Haq, 2014). The different hypotheses that could cause the fertilization of the ocean need to be tested for the Weissert positive CIE. A biocalcification crisis in both platform and pelagic settings has been inferred from carbonate platform drowning around the early-late Valanginian (Weissert et al., 1998; Wortmann and Weissert, 2000; Föllmi et al., 2006), and a nannoconid decline predating the positive CIE has been identified (Channell et al., 1993; Bersezio et al., 2002; Erba and Tremolada, 2004; Gréselle et al., 2011; Barbarin et al., 2012).

This study aims to reconstruct the paleoceanographic conditions around the Weissert Event on the central Moroccan margin, which was located on the south Tethyan margin during the Cretaceous. Calcareous nannofossil abundances and accumulation rates together with their assemblages were used to quantify changes in surface-water nannofossil production and fertility conditions. Nannofossil samples were collected from three geological successions located on a proximal-distal transect: two onshore sections (Zalidou and Aït Hamouch belonging to the Essaouira-Agadir Basin, EAB) and an offshore DSDP Hole 416A (east Atlantic Ocean). The paleogeographic context of the onshore sections was defined from a sedimentological analysis done at the scale of the EAB. The time framework was based on ammonite (only for the onshore sections) and calcareous nannofossil biostratigraphy, and carbon-isotope stratigraphy. The transect allowed to better constrain the variations of continental nutrient flux, upwellings that were present on the NW African margin during the Early Cretaceous due to active trade winds considering atmospheric circulation models from Price et al. (1995) and Poulsen et al. (1998), and calcareous nannofossil production.

2. Geological setting

The Essaouira-Agadir Basin (EAB) is located in southwest Morocco and corresponds to the westernmost part of the High Atlas fold belt, bounded by 9º55' to 9º20' W and 30º30' to 31º05' N. The basin is bordered to the north by the Jebilet Massif and Doukkala Plateau (Paleozoic basements), to the south by the plain of Souss (Neogene basin), and to the east by the High Atlas (Fig. 1). The EAB presently constitutes part of the Atlantic passive margin which is considered one of the oldest existing passive margins (Stets and Wurster, 1982; Sahabi et al., 2004). The EAB extends offshore until the western limit of the continental margin (Frizon de Lamotte et al., 2008). During the Cretaceous, the central Moroccan margin which includes the EAB occupied a paleogeographic location on the south Tethyan margin, between paleo-latitudes ~ 15°N and ~ 22°N (Fig. 2). Until the opening of the South Atlantic (Valanginian) and its connection with the Central Atlantic (early Albian), the Tethys Ocean included what is presently the Central Atlantic. Therefore, the geological evolution of the Atlantic-Tethyan passive margin controlled the development of the EAB (Ellouz et al., 2003). Two sections in the EAB, namely Zalidou and Aït Hamouch, were selected for the study of calcareous nannofossils. The Zalidou section is located 45 km north of Agadir (30°54'23"N; 9°39'48"W; Fig. 1B), whereas the Aït Hamouch section is located ~25 km NNW of Agadir (30°36'54"N; 9°42'14"W). The Aït Hamouch section is composed of two adjacent sections, only 0.6 km apart from each other. The primary section, denoted "AH", was not accessible in its middle part (between 32 and 42 m). Accordingly, the nearby "ATH" section was studied and correlated using ammonite biostratigraphy and sedimentological discontinuities. Moreover, calcareous nannofossils were studied in the offshore succession DSDP Leg 50 Hole 416A (Fig. 1A). Additional sections were used in this paper to improve the precision of the ammonite biostratigraphy and the sedimentological framework (Fig. 1B), although these sections will not be discussed in detail herein as this is beyond the scope of this paper.

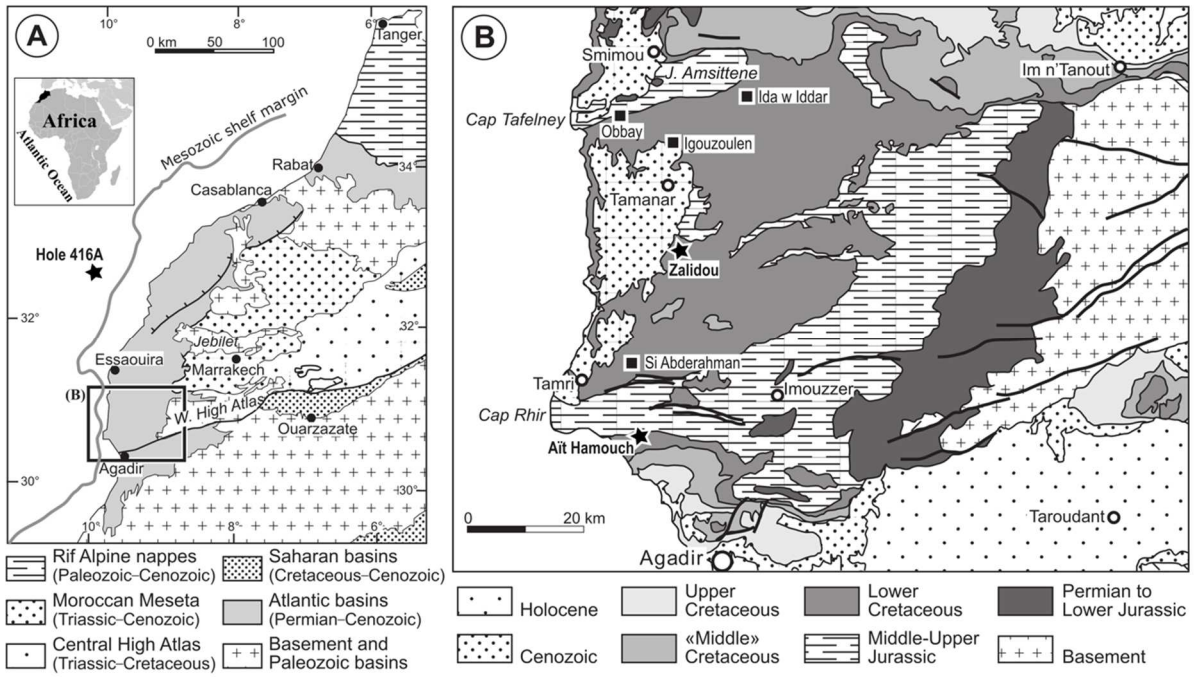

Fig. 1. Location of the study area in SW Morocco, modified from Ouajhain et al. (2009). (A) Location of the central Moroccan margin including the Essaouira-Agadir Basin and DSDP Hole 416A (not to scale). Approximate location of the Mesozoic shelf margin from Tari and Jabour (2013). (B) Geological sketch including the location of the sections used in this study (square shape). The successions studied for their calcareous nannofossil assemblages (Zalidou, Aït Hamouch, and Hole 416A) are identified in "bold" font and by a "star" sign.

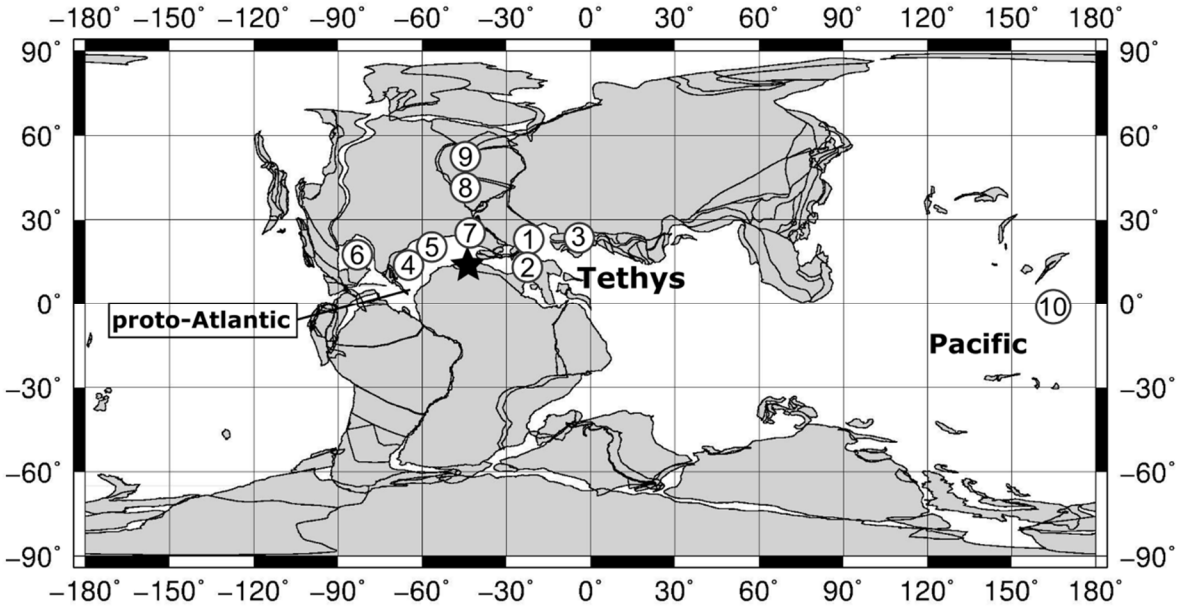

Fig. 2. Paleogeographic map of the Valanginian (136 Ma) showing the location of the central Moroccan margin (star shape). The "white circles" correspond to the location of basins/successions where calcareous nannofossils of the Weissert Event were investigated: Tethyan Realm, (1) Vocontian Basin (France) (Duchamp-Alphonse et al., 2007, 2014; Gréselle et al., 2011; Barbarin et al., 2012; Mattioli et al., 2014), (2) Lombardy Basin (Italy) (Bersezio et al., 2002; Erba and Tremolada, 2004), and (3) Moesian Platform (south and east Carpathians-Romania) (Melinte and Mutterlose, 2001); western and central Atlantic, (4) DSDP 534A (Blake

Bahama basin, NE Florida) and (5) DSDP 603B (east Florida) (Bornemann and Mutterlose, 2008), and (6) DSDP 535 (SE Gulf of Mexico) (Kessels et al., 2006); Boreal Realm, (7) ODP 638 (NW Iberian Peninsula) (Kessels et al., 2006), (8) BGS 81/43 (southern North Sea Basin, east England) (Williams and Bralower, 1995; Kessels et al., 2006), and (9) east Greenland Basin (NE Greenland) (Pauly et al., 2012); western Pacific, (10) ODP 1149B (Nadezhda Basin) (Lozar and Tremolada, 2003). Construction from http://www.odsn.de (made from the datafiles of Hay et al. (1999)).

2.1 Ammonite zonal framework for the late Berriasian-early Hauterivian interval of the EAB

The systematic revision and identification of ammonites sampled at Zalidou and Aït Hamouch sections are being prepared as a separate paper and were part of a chapter in Shmeit's PhD thesis (2021), in which paleontological comments and ranges of ammonite taxa are provided. The standard ammonite zonation for the Mediterranean Province (Tethyan Realm, Reboulet et al., 2018) is applied here. Only two regional units are added, namely *Neocomites subtenuis* and *Busnardoites campylotoxus* local subzones, to make more accessible the comparisons with previous works made in this Moroccan area by Wippich (2001, 2003) and Ettachfini (2004). The ammonite (sub-)zones are interval (sub-)zones defined by the first appearance datum (FAD) of two successive ammonite-indices. Hereafter will be used the following abbreviations: standard zone = StZ, standard subzone = StSz, and local subzone = LSz.

The base of the *Thurmanniceras pertransiens* StZ, and therefore the lower boundary of the Valanginian, is placed by the FAD of the index-species (Kenjo et al., 2021). As it is relatively rare at Zalidou and Aït Hamouch, the base of the zone can be placed at the first records of *Neocomites premolicus* (Ettachfini, 2004; Reboulet et al., 2018). Due to the rarity of the index-species, the base of the *N. neocomiensiformis* StZ is identified at Zalidou and Aït Hamouch sections by the first occurrence (FO) of *Neocomites subtenuis*, as its appearance is contemporaneous with that of *N. neocomiensiformis* in SE Spain (Company and Tavera, 2015). Above the *N. subtenuis* LSz, the upper part of the *N. neocomiensiformis* StZ is characterized by

187 the *Busnardoites campylotoxus* LSz, for which the base is placed at the FO of its relatively
188 abundant index-species at Zalidou and Aït Hamouch. The base of the *Karakaschiceras*
189 *inostranzewi* StZ is placed at the FO of its index species. In both sections, *Saynoceras*
190 *verrucosum*, index species of the *S. verrucosum StZ*, was not found. Other ammonite markers
191 of the basal part of this zone, as *Valanginites ventrotuberculatus*, were also not observed.
192 Consequently, at Zalidou, the base of the *S. verrucosum* StZ, and so the base of the late
193 Valanginian, are placed at the FO of *Karakaschiceras pronecostatum* that is the index-species
194 of the second subzone of the *S. verrucosum* StZ. At Aït Hamouch, very few specimens of some
195 taxa that could be restricted to the *S. verrucosum* StZ are recorded in a single layer (AH89) with
196 the FO of *Neocomites peregrinus* allowing to identify the base of the *N. peregrinus* Stz. Thus,
197 the ammonite assemblage could be interpreted as a result of a condensed lithology. In this layer,
198 there are also few doubtful specimens of *K. inostranzewi?*; their preservation could indicate
199 that they have been reworked. At Zalidou, *N. peregrinus* was also observed allowing to place
200 the base of the zone. In this section, the *Olcostephanus nicklesi* StSz is identified by the
201 occurrence of the genus *Himantoceras* (see Reboulet, 1996). The *O. nicklesi* StSz is not
202 recognized at Aït Hamouch. The base of the *Criosarasinella furcillata* StZ and that of the
203 *Teschenicerasc callidiscum* StSz are identified in both sections. The base of the *Acanthodiscus*
204 *radiatus* StZ, and thus the base of the Hauterivian (see Mutterlose et al., 2020), are placed at
205 the FO of *Breistrofferella castellanensis* and that of *Acanthodiscus radiatus* at Zalidou and Aït
206 Hamouch, respectively.

207 **2.2 DSDP Hole 416A**

208 DSDP Leg 50 Hole 416A was drilled ~180 km NW of Essaouira (32°50'10.7"N;
209 10°48'03.6"W) at a water depth of 4201 m in the eastern Atlantic (Fig. Supp. 1). The Berriasian
210 to Hauterivian sediments consist of a turbidite succession deposited in a lowermost continental
211 rise environment (Lancelot et al., 1980). The Valanginian interval was identified onboard from

cores 48 to 14, between –1540 and –1222 meters below seafloor (mbsf) (Čepek and Gartner, 1980; Sliter, 1980). The detailed lithology of Hole 416A was described by Lancelot et al. (1980). Briefly, the Berriasian and early Valanginian were assigned to lithological unit VII (from –1624 to –1430 mbsf, cores 57 to 37), characterized by alternating siliciclastic and carbonate turbidites. The lithology displays quartz-rich siltstone and mudstone cycles alternating with hard micritic and calpionellid-rich limestones. A prominent change in lithology above –1430 mbsf characterizes the shift to the overlying lithological unit VI (from to –1430 to –880 mbsf, cores 36 to 7). This change is identified by an abrupt decrease in carbonate deposition and a subsequent increase in terrigenous input, with siliciclastic terrigenous turbidites replacing the calcareous turbidites. The lithology change was regarded as a classical example of the mid-Valanginian platform drowning (Schlager, 1980). Lithological unit VI spans the rest of the Valanginian and builds up to the Hauterivian (Lancelot et al., 1980; Schlager, 1980). The lithology shows graded calcareous and siliciclastic cycles, from siltstone or fine sandstone to mudstone.

3. Materials and methods

The onshore successions (Zalidou and Aït Hamouch) span the late Berriasian to early Hauterivian covering the entire Valanginian. The offshore DSDP Leg 50 Hole 416A spans the Valanginian stage (Čepek and Gartner, 1980). Samples for calcareous nannofossils, calcium carbonate content, and carbon-isotope analyses were collected from different lithologies (except sandstones). The sampling interval was on average 0.3 m in Zalidou, 0.5 m in Aït Hamouch, and 5 m in Hole 416A. Both macrofossils and nannofossil smear slides are curated at the Collections de Géologie de l'Observatoire des Sciences de l'Univers de Grenoble (OSUG), with an appropriate UJF-ID number. "OSUG-COLLECTIONS" is a database of rocks, minerals, and fossils (https://web.collections.osug.fr, OSUG, UGA; doi:10.5072/OSUG-COLLECTIONS.all).

3.1 Sedimentological analysis

Sedimentological analysis was based on sections located in the southern and central parts of the EAB (Fig. 1B). Observations were made both in the field and under microscope. All sedimentary features (lithology, peculiar surfaces, sedimentary figures, faunal content, and bioturbation) were observed and recorded in the field. Limestone beds, mainly in the lower Valanginian series, were also sampled for microfacies analysis. We used the classification defined by Dunham (1962).

3.2 Calcareous nannofossils

Biostratigraphic and paleoenvironmental analyses of the Zalidou and Aït Hamouch sections were based on 85 and 54 samples (Supplementary Table), respectively, from calcareous claystone to limestone. For Hole 416A, 44 samples were investigated.

Smear slides were prepared using a random settling technique developed by Beaufort et al. (2014) and modified by Menini et al. (2019). Only 17 samples from the Aït Hamouch "AH section" were prepared using the random settling technique of Geisen et al. (1999) (see Supplementary Table). Both techniques allow the determination of the nannofossil absolute abundance (nannofossils/gram of rock) using the equations presented in the Supplementary Table. A comparison between both techniques for absolute abundance quantification has not been done yet. Studies comparing other slide preparation techniques have shown that nannofossil proportions can be reliably determined regardless of the technique (Bordiga et al., 2015; Lupi et al., 2016).

Nannofossils were observed using a polarizing light microscope (Leica "DM2500 P") at 1000x magnification. Five hundred specimens per slide, both coccoliths and nannoliths, were generally counted in a variable number of fields of view (a mean of 52 for Zalidou, 80 for Aït Hamouch, and 39 for DSDP Hole 416A). All nannofossils with at least more than half of the specimen preserved were counted. In few samples (4 from Zalidou and 3 from Aït Hamouch),

characterized by low abundance of nannofossils (approx. 1–2 specimens/4 fields of view), ~ 350–400 specimens were counted (Supplementary Table). In addition, two longitudinal random transverses (200 fields of view per transverse) were scanned after each counting for rare species that could be of biostratigraphic importance. To improve the biostratigraphic schemes whenever needed, scanning ~8–12 random longitudinal transverses was done on additional samples not counted (5 from Zalidou, 1 from Aït Hamouch, and 11 from Hole 416A).

The taxonomic frameworks of Perch-Nielsen (1985), Bown and Young (1998), and Nannotax3 (Young et al., 2017) were followed. For nannoconids, the work of Deres and Achéritéguy (1980) was followed. The calcareous nannofossil zonation applied to the investigated sections were the NC and NK zones of Bralower (1987) and Bralower et al. (1989, 1995), modified from Roth (1978). This zonation scheme was selected because of its applicability to low-latitude Tethyan continental margins and Atlantic oceanic settings (Bralower et al., 1995; Bown, 2005; Bornemann and Mutterlose, 2008). The biostratigraphic scheme (CC zones and subzones) of Sissingh (1977), modified by Perch-Nielsen (1979, 1985) and Applegate and Bergen (1988), was also applied to the studied sections because it allows subdividing the early Valanginian. This zonal scheme uses taxa with cosmopolitan distribution and Tethyan affinities, and it relies on the first occurrence (FO) of *Eiffelithus* taxa (*E. windii* and *E. striatus*) for subzone divisions during the Valanginian stage.

Nannofossil preservation was evaluated following the classes defined by Roth and Thierstein (1972) and modified by Roth (1983). Nannofossil absolute abundances are controlled by the nannoplankton biomass, preservation, and sedimentation rate. Nannofossil accumulation rates (nannofossils/m^2/yr) were calculated to cancel the sedimentation rate effect (see formula in Supplementary Table). The duration of the different phases of the positive CIE from Martinez et al. (2015) were used to determine the sedimentation rates in the studied sections. These authors provided an improved age model for the Valanginian-Hauterivian

boundary using astrochronology, and acquired absolute age durations for the different phases of the positive CIE. The $\delta^{13}C_{carb}$ values and the ammonite zonation of the onshore sections (Zalidou and Aït Hamouch) were correlated with those of Martinez et al. (2015).

For each nannofossil taxon (or group of combined taxa) the absolute abundance (AA), the relative abundance (RA), and the accumulation rate (AR, only for the Zalidou and Aït Hamouch sections) were calculated. In addition, the nannofossil total absolute abundance (NTAA) and the nannofossil total accumulation rate (NTAR, for Zalidou and Aït Hamouch sections) were calculated, corresponding to the entire nannofossil assemblage. To consider the inherent counting uncertainty, binomial proportion confidence intervals for relative abundances were computed based on the 'exact' Clopper–Pearson method using the PAST software (Hammer et al., 2001; Suchéras-Marx et al., 2019). Additionally, diversity indices were calculated. *Nannoconus* spp. were excluded from the calculation of sample diversity indices, absolute/relative abundances, and accumulation rates of other taxa because of their uncertain biological affinity (Aubry et al., 2005). The counting and the different calculation formulae are given in the Supplementary Table.

3.3 Calcimetry and carbon isotopes

The calcium carbonate content was measured on 117 and 56 bulk rock samples from Zalidou and Aït Hamouch sections, respectively (Supplementary Table). For Aït Hamouch, analyses were done on samples from the "AH" section. Additionally, 88 samples from DSDP Hole 416A were measured (Supplementary Table). The $CaCO_3$ content was determined using the carbonate bomb technique (Müller and Gastner, 1971). For the calculation of the calcium carbonate percentage, see Appendix A in Peybernes et al. (2013).

Carbon stable isotope analysis was performed on the same samples as for the calcium carbonate content at the stable isotope laboratories of the Institute of Earth Surface Dynamics of the University of Lausanne, using a Thermo Fisher Scientific Gas Bench II carbonate

preparation device connected to a Delta Plus XL isotope ratio mass spectrometer. The CO_2 extraction was done at 70°C. The carbon stable isotope ratios were reported in the delta (δ) notation as the per mil (‰) relative to the Vienna Pee Dee belemnite standard (VPDB), where $\delta = (R_{sample} - R_{standard})/R_{standard}$ and $R = {}^{13}C/{}^{12}C$. The $\delta^{13}C_{carb}$ values were standardized relative to the international VPDB scale by calibration of the reference gases and working standards with international reference materials NBS 18 (carbonatite, $\delta^{13}C = -5.01$ ‰) and NBS 19 (limestone, $\delta^{13}C = +1.95$ ‰). Analytical uncertainty (1 sigma), monitored by replicate analyses of the international calcite standard NBS 19 and the laboratory standard Carrara Marble ($\delta^{13}C = +2.05$ ‰) was not greater than ±0.05‰ for $\delta^{13}C$.

4. Results

4.1 Summary of the Valanginian sedimentary evolution

Geological sections indicated in "bold" font hereafter, correspond to sections that have been investigated for calcareous nannofossils in the present study. Detailed analysis allowed the identification of several sequences. Three main stages can be recognized in the Valanginian sedimentary evolution of the EAB.

1. The top of the Berriasian carbonate shelf is marked by a karstified surface in the northern sections. The overlying lower Valanginian succession (8-15 m) is dominated by marlstone and thin limestone beds (Fig. 3). It shows a thinning-upward, then thickening-upward trend. In the thinning-upward lower part, ammonites, belemnites, plicatulids, and brachiopods dominate. They are also associated with ostreids, *Trichites* sp., pectinids, and with sea-urchins at the base (Fig. 3). Microfacies show mudstone to wackestone textures containing mainly echinoids, bivalves, and agglutinated foraminifers. The fauna indicates an outer shelf depositional environment that represents the maximum depositional depth for the early Valanginian period. In the upper part of the lower Valanginian succession, limestone beds are more abundant and sandstone beds appear in the south (**Aït Hamouch**). The macrofauna is

337 composed of ammonites, belemnites, brachiopods, oysters, and plicatulids, with subordinate
338 regular and irregular sea-urchins, crinoids, serpulids, and locally corals and bone fragments
339 (Fig. 3). Compared with the lower part, this assemblage indicates a shallower depositional
340 depth. Microfacies analysis reveals wackestone textures containing agglutinated foraminifers,
341 brachiopods, echinoids, and benthic foraminifers. Several discontinuities (erosion, karsted
342 surfaces) indicate the existence of three or four depositional sequences, and support a marked
343 shallowing-upward trend that culminated in the late early Valanginian. The Obbay section
344 exhibits a very reduced lower Valanginian succession (3 m), mainly made of limestone beds
345 alternating with thin marlstone interbeds (Fig. 3). Limestones show a wackestone texture
346 containing abundant phosphate-rich glauconitic oolites and are frequently capped by iron-rich
347 hardgrounds. The causes of condensation of this series are discussed in section 5.1.
348 2. The lower part of the upper Valanginian series (5-15 m) is mainly made of marlstone,
349 thin limestone beds, sandy marlstone, and sandy limestone. The sandy beds are more abundant
350 to the north and east (Fig. 3). The succession shows a thinning-upward trend, locally overlain
351 by a thickening-upward series, interrupted by a major erosion period (D7) that removed one
352 depositional sequence in many sections (Fig. 3). It contains an outer shelf to hemipelagic
353 macrofauna (ammonites, belemnites, brachiopods, and plicatulids), although small bivalves and
354 wood fragments are locally found. The upper Valanginian succession is interpreted as a
355 transgressive-regressive sequence, the top of which is frequently eroded. The maximum
356 depositional depth reached a rather deep outer shelf environment during the “middle” late
357 Valanginian.
358 3. The uppermost Valanginian series (8-22 m) is mainly composed of marlstone, thin
359 limestone beds, sandy limestone to the south, and of sandy marlstone and calcareous sandstone
360 to the north. The succession exhibits an overall thinning-, then thickening-upward trend. The
361 macrofauna is dominated by ammonites, belemnites, brachiopods, plicatulids, and serpulids,

locally associated with gastropods and wood fragments. To the north and east of the basin, the uppermost Valanginian deposits are made of sandstone (**Zalidou**) locally showing current ripples, Hummocky Cross Stratification (HCS), and low angle lamination (Ida w Iddar) (Fig. 3), interpreted as foreshore deposits. This succession is thus interpreted as a transgressive-regressive sequence reaching an outer shelf environment to the south. The thick overlying Hauterivian marlstone represent a new, major sea level rise (Ferry et al., 2007).

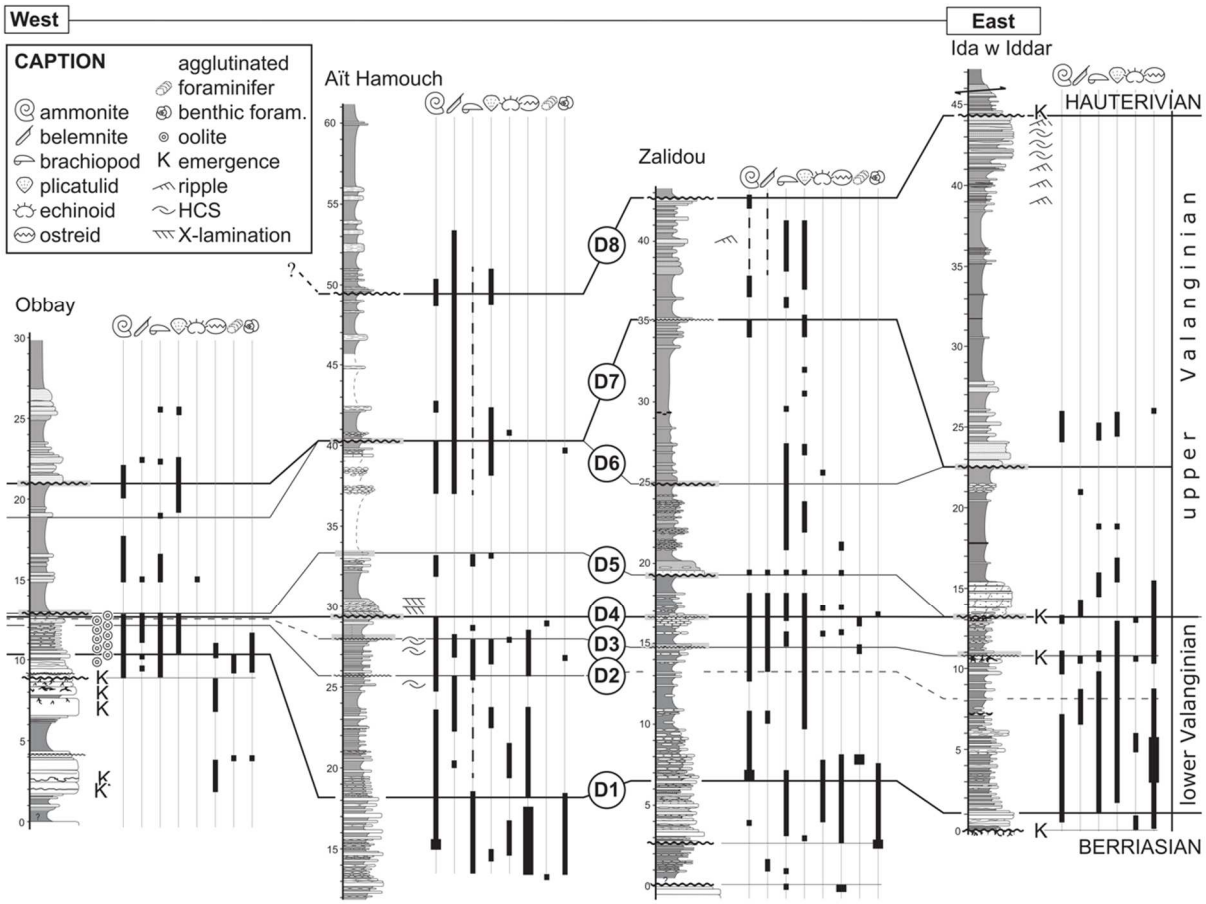

Fig. 3. Main sedimentary features, faunal assemblages, and discontinuities (D1 to D8) of some Valanginian sections in the Essaouira-Agadir Basin. Location of sections is shown in Fig. 1B.

4.2 Calcareous nannofossil biostratigraphy

The identified biozones of Bralower et al. (1995) and Sissingh (1977) are illustrated for the Zalidou section (Fig. 4), Ait Hamouch section (Fig. 5), and Hole 416A (Fig. 6). Secondary nannofossil bioevents were also observed (Figs. 4-6). Nannofossil zonal and subzonal markers are illustrated in Figure 7.

A gradual size transition was observed between *Eiffelithus windii* and *E. striatus* (Applegate and Bergen, 1988; Bralower et al., 1989; Bown and Concheyro, 2004), making a proper differentiation difficult. Coccoliths with the length of their long-axes greater than 6.0 µm and with a relatively wide central area (almost 2/3 or greater of coccolith length) were identified in this study as *E. striatus* (Fig. 7).

Additionally, a new calcareous nannofossil biostratigraphy is proposed for Hole 416A. Čepek and Gartner (1980) dated the interval between cores 48-1 and 7-1 (~ –1530 to –1000 mbsf) to the early Valanginian-late Hauterivian based on calcareous nannofossil biostratigraphy. The LO of *R. wisei* was observed in this study in core 11-4 (–1200 mbsf; Fig. 6). In the Zalidou and Aït Hamouch sections, the LO of *R. wisei* was observed in the early late Valanginian (lower and upper *N. peregrinus* StZ in Zalidou and Aït Hamouch, respectively; Figs. 4, 5). Also, our results demonstrate that the Valanginian stage extends to core 9-3 (–1122 mbsf) based on the LO of *T. verenae* (top NK3B Subzone). In the onshore sections, the top of the NK3B Subzone ends in the late Valanginian (uppermost *N. peregrinus* StSz). The LO of *T. verenae* was also observed at a similar stratigraphic interval both in the Vocontian Basin (Duchamp-Alphonse et al., 2007; Gréselle et al. 2011) and in the Subbetic Basin (Aguado et al. 2018). Therefore, we can assume that the top of the studied interval at Hole 416A records the late Valanginian, but not the latest Valanginian.

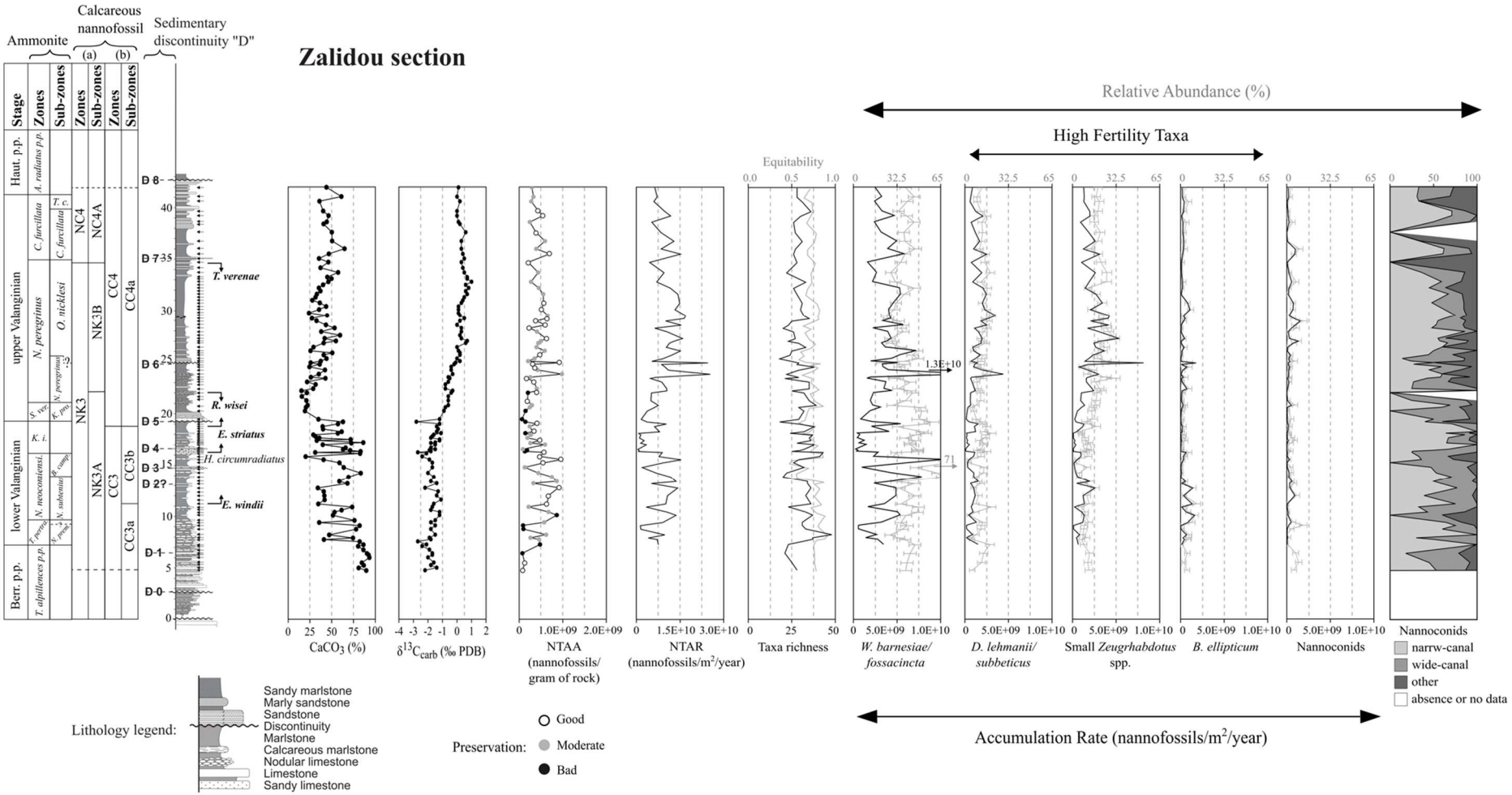

Fig. 4. Calcareous nannofossil and geochemical results in the Zalidou section. Sample locations are indicated by the arrow signs. The recognized stages are plotted with, the ammonite biostratigraphy (zones/subzones) following the ammonite standard zonation of the Mediterranean Province from Reboulet et al. (2018), calcareous nannofossil biostratigraphy (zones/subzones) following the (a) NC and NK zonation of Bralower et al. (1989, 1995) and (b) CC zonation of Sissingh (1977) modified by Applegate and Bergen (1988), sedimentary discontinuities (D0 to D8), and lithology. Calcareous nannofossil first and last occurrences are included; taxa indicated in "bold" font are used in the biostratigraphic schemes (a)

and (b), and those in "normal" font correspond to the secondary bioevents. Binomial proportion confidence intervals are included for the nannofossil relative abundances using the 'exact' Clopper–Pearson method. The proportion of narrow- and wide-canal nannoconids within the nannoconid population are also shown, "other" nannoconids include specimens whose central-canal was not recognizable. Abbreviations: Berr., Berriasian; Haut., Hauterivian; *T. pertra.*, *T. pertransiens*; *N. prem.*, *N. premolicus*; *N. neocomiensi.*, *N. neocomiensiformis*; *B. camp.*, *B. campylotoxus*; *K. i.*, *K. inostranzewi*; *S. ver.*, *S. verrucosum*; *K. pro.*, *K. pronecostatum*; *T. c.*, *Teschenicera callidiscum*; NTAA, nannofossil total absolute abundance and NTAR, nannofossil total accumulation rate.

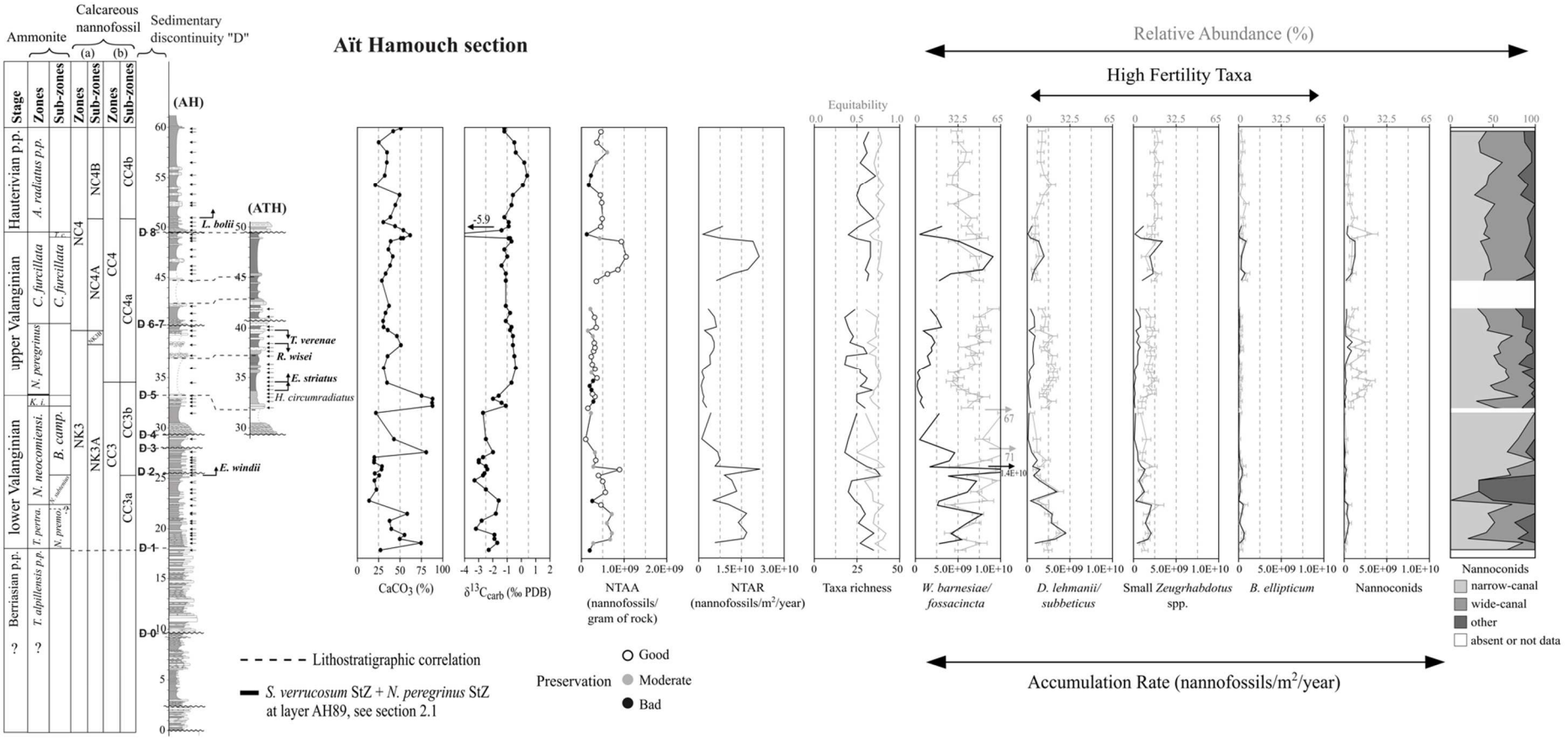

Fig. 5. Calcareous nannofossil and geochemical results in the Aït Hamouch section, same caption and lithology legend as for Fig. 4. Calcareous nannofossil results from "AH" section are separated from "ATH" section (see section 2).

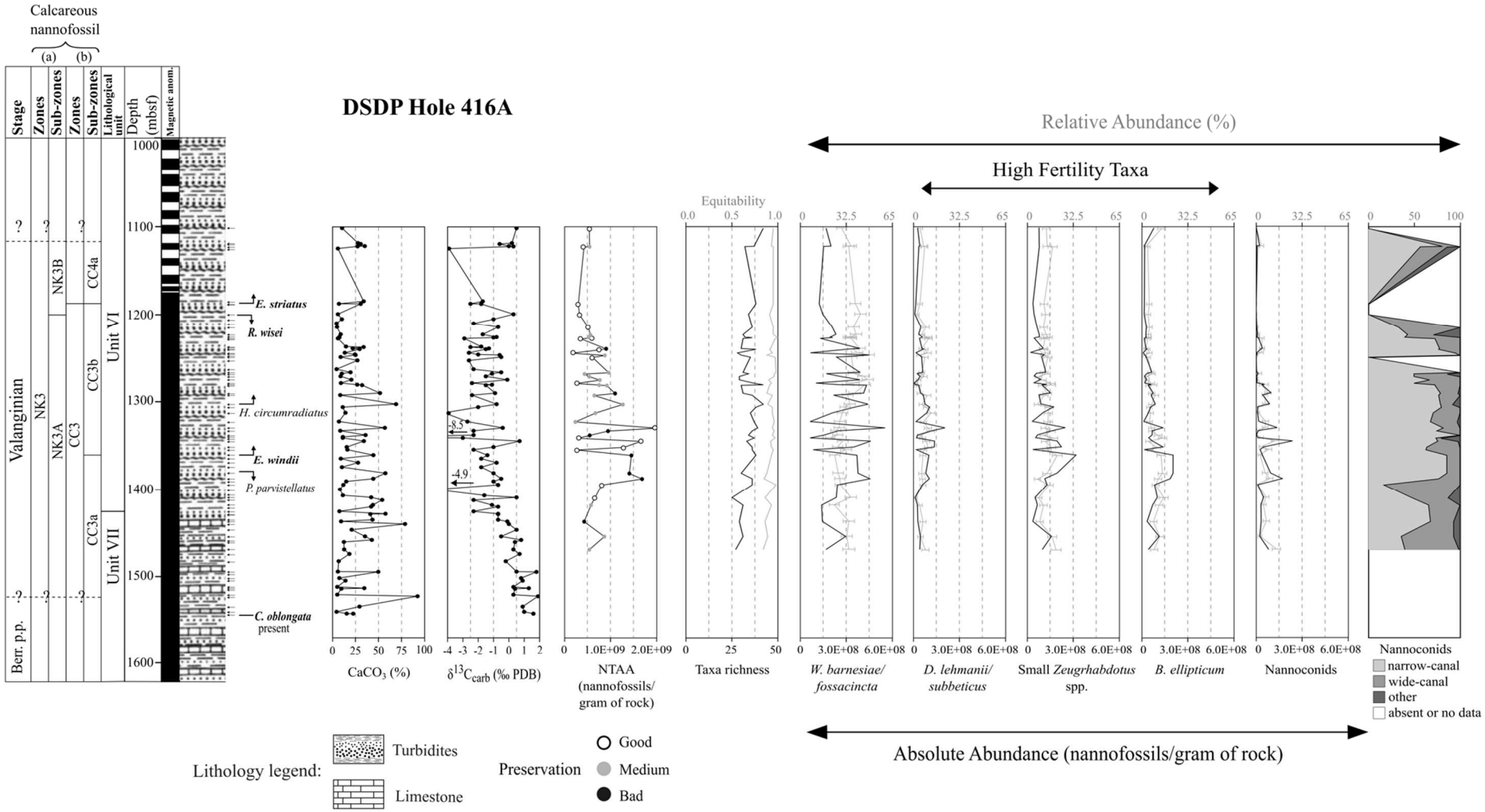

Fig. 6. Calcareous nannofossil and geochemical results in the DSDP Hole 416A. Sample locations are indicated by the arrow signs. The recognized stage is plotted with, the calcareous nannofossil biostratigraphy (zones/subzones) following the (a) NC and NK zonation of Bralower et al. (1989, 1995) and (b) CC zonation of Sissingh (1977) modified by Applegate and Bergen (1988), and lithology. Calcareous nannofossil first and last occurrences are included; taxa indicated in "bold" font are used in the biostratigraphic schemes (a) and (b), and those in "normal" font correspond to the secondary bioevents. Binomial proportion confidence intervals are included for the nannofossil relative abundances using the 'exact' Clopper–Pearson method. The proportion of narrow- and wide-canal nannoconids within the nannoconid population are also shown, "other" nannoconids include specimens whose central-canal was not recognizable. Abbreviations: Berr., Berriasian; magnetic anom., magnetic anomalies; and NTAA, nannofossil total absolute abundance.

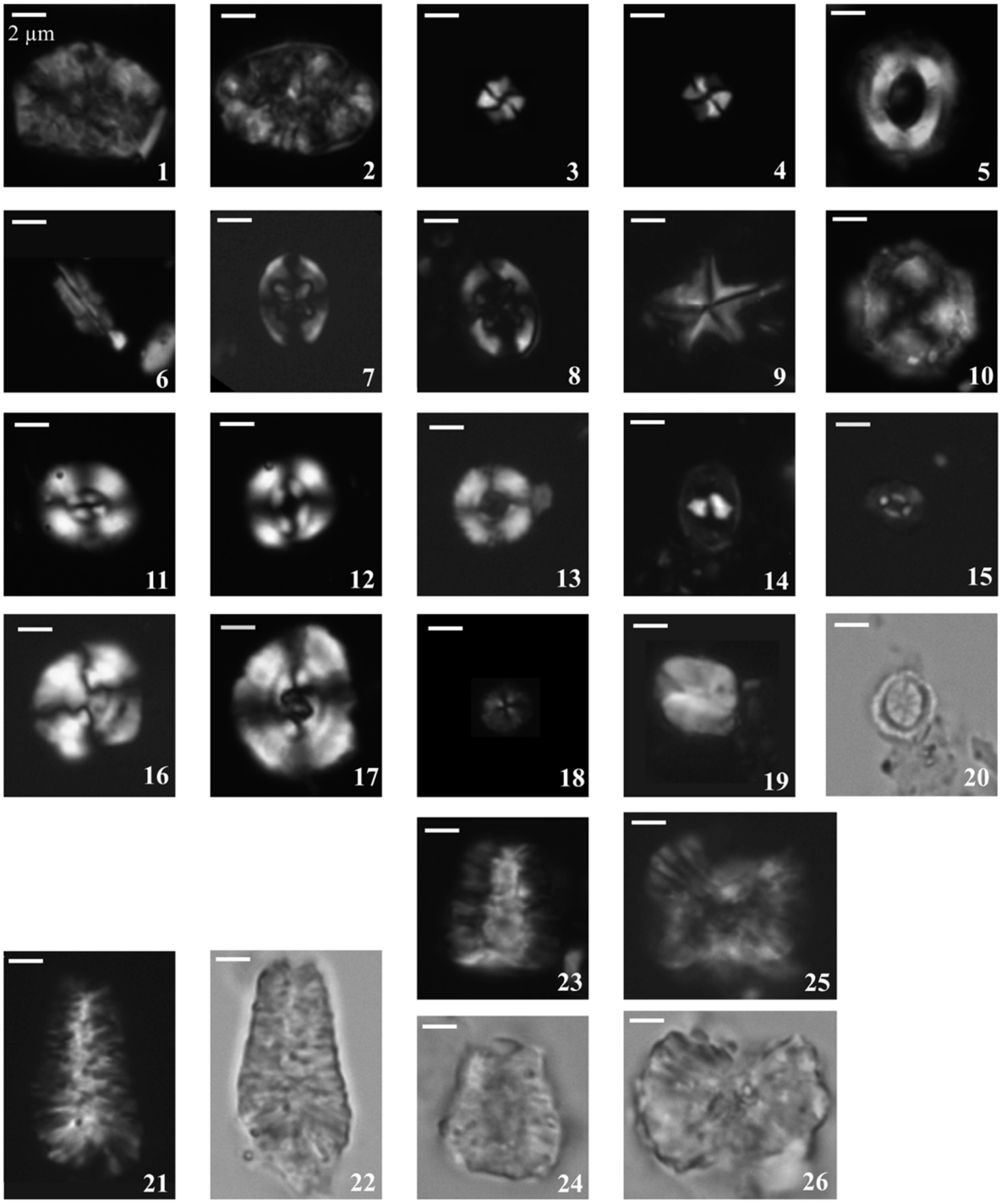

Fig. 7. Photomicrographs of the selected nannofossil species (XPL: cross-polarized light; PPL: plane-polarized light). 1, *Calcicalathina oblongata*, side view, XPL, sample Za43c; 2, *Calcicalathina oblongata*, top view, XPL, sample Za49b; 3, *Rucinolithus wisei*, XPL, sample Za27a; 4, *Rucinolithus wisei*, XPL, sample Za27a, same specimen rotated ~90º; 5, *Tubodiscus verenae*, XPL, sample 416A 21R2w 103-104; 6, *Lithraphidites bollii*, XPL, sample AH112a; 7, *Eiffellithus windii*, XPL, sample 416A 10R2w 144-145; 8, *Eiffellithus striatus*, XPL, sample Za53a; 9, *Polycostella parvistellatus*, XPL, sample 416A 49R1w 124-125; 10, *Haqius circumradiatus*, XPL, sample ATH2d; 11, *Watznaueria barnesiae*, XPL, sample Za28a; 12, *Watznaueria fossacincta*, XPL, sample Za39a; 13, *Diazomatolithus lehmanii*, XPL, sample Za32b; 14, *Zeugrhabdotus erectus*, XPL, sample 416A 9R3w 135-136; 15, *Biscutum ellipticum*, XPL, sample Za32a; 16, *Watznaueria biporta*, XPL, sample Za32a; 17, *Watznaueria britannica*, XPL, sample Za39c; 18, *Discorhabdus ignotus*, XPL, sample Za39d; 19, *Assipetra*

infracretacea, XPL, sample Za32a; 20, *Rotelapillus crenulatus*, PPL, sample 416A 47R1w 76-77; 21, *N. steinmannii subsp. steinmannii*, XPL, sample ATH2h; 22, *N. steinmannii subsp. steinmannii*, PPL, sample ATH2h, same specimen; 23, *N. kamptneri subsp. minor*, XPL, sample ATH2f; 24, *N. kamptneri subsp. minor*, PPL, sample ATH2f, same specimen; 25, *N. globulus subsp. globulus*, XPL, sample ATH2f; 26, *N. globulus subsp. globulus*, PPL, sample ATH2f, same specimen.

4.3 Calcareous nannofossil assemblages

The majority of studied samples show good to moderate preservation of calcareous nannofossils with minor dissolution and recrystallization (Fig. 8). Note that the delicate structures of coccoliths are still visible. Highly dissolved and recrystallized coccoliths were limited to 14–18 % of all the samples.

Following the abundance classes defined by Erba and Quadrio (1987), calcareous nannofossils are common (10–20 specimens per field of view) in the majority of the studied samples. The calcareous nannofossil assemblage is dominated by eight and nine groups of taxa in the onshore and offshore successions, respectively, illustrated in Figure 7. Altogether, they constitute on average 81 % of the total assemblage at Zalidou, 88 % at Aït Hamouch, and 79 % at Hole 416A. They are: *Watznaueria barnesiae/fossacincta*, *Diazomatolithus lehmanii/subbeticus*, small *Zeugrhabdotus* spp., *Biscutum ellipticum*, nannoconids, and to a lesser extent *Discorhabdus ignotus*, other *Watznaueria* species (*W. biporta* and *W. britannica*), and *Assipetra infracretacea*. *Rotelapillus crenulatus* are negligible in both onshore sections, but not at Hole 416A. The reader is referred to the Supplementary Table for more details.

In this study, *Diazomatolithus lehmanii* and *Diazomatolithus subbeticus* were combined since they are considered as morphological variants (Grün and Allemann, 1975). The small *Zeugrhabdotus* spp. in this study correspond to *Zeugrhabdotus* with long axis ≤5 μm combined with *Zeugrhabdotus erectus*. Finally, *W. barnesiae* and *W. fossacincta* were merged since they are considered to be morphological variants (Bornemann and Mutterlose, 2006).

The nannoconid group is mainly represented in all studied successions by three taxa, *N. steinmannii* corresponding to narrow-canal, and *N. kamptneri* and *N. globulus* both

corresponding to wide-canal (see Supplementary Table). These three taxa constitute on average ~80 % of the total nannoconid population in both onshore sections and ~94 % at Hole 416A. Additionally, *N. steinmannii* is the dominant taxon within the total nannoconid population in all three successions (see Supplementary Table).

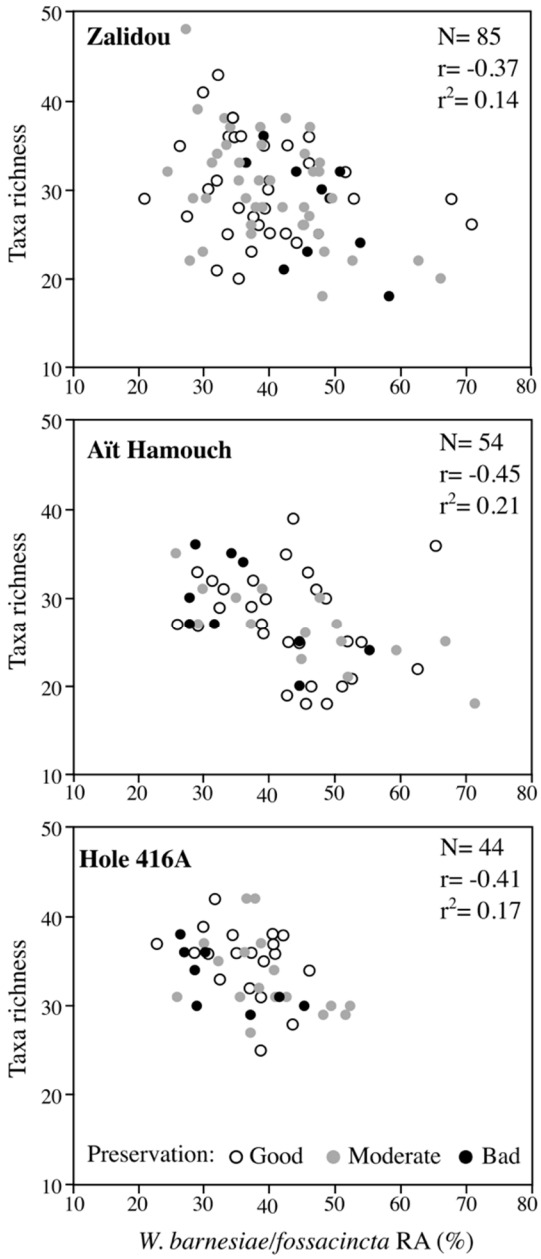

Fig. 8. Plot of *W. barnesiae/fossacincta* relative abundance (RA, %) and taxa richness in Zalidou, Aït Hamouch, and Hole 416A samples. Preservation classes follow the classes defined by Roth and Thierstein (1972) and modified by Roth (1983). N is the total number of samples, r and r^2 are the correlation coefficients.

4.3.1 Calcareous nannofossil absolute abundance and accumulation rate

Four and three intervals with different sedimentation rates were identified throughout the Valanginian stage in Zalidou and Aït Hamouch, respectively (see Supplementary Table). Thus, allowing the calculation of the nannofossil total accumulation rate (NTAR, nannofossils/m^2/year). It was not possible to calculate sedimentation rates, and then NTAR, for Hole 416A because the large scatter in $\delta^{13}C_{carb}$ (Fig. 6) hindered identifying possible correlation points with the $\delta^{13}C_{carb}$ curve from Martinez et al. (2015).

The average nannofossil total absolute abundance (NTAA, nannofossils/gram of rock) is higher offshore compared to onshore, and the average NTAR is higher at Zalidou than at Aït Hamouch (Figs 4-6, see also Supplementary Table). In both Zalidou and Aït Hamouch successions (Figs. 4, 5), the NTAR is high in the early Valanginian. Afterwards, NTAR decreases and minimal values are recorded around the early-late Valanginian transition (*K. inostranzewi* to *S. verrucosum* StZ, upper NK3A and upper CC3b subzones). Upwards, in the late Valanginian, NTAR gradually increases in both successions. It reaches maximal values within the *N. peregrinus* StZ at Zalidou (Fig. 4), followed by a slight decrease during the rest of the succession. At Aït Hamouch, NTAR values higher than that of the early Valanginian are recorded within the *C. furcillata* StZ (Fig. 5). In both successions, NTAR reflects an amplification of NTAA with very similar trends (Figs. 4, 5), which implies that the sedimentation rate does not significantly affect the NTAA. At Hole 416A, NTAA is low in the lower NK3A and CC3a subzones, and increases during the mid-NK3A and upper CC3a to lower CC3b subzones (Fig. 6). Thereafter, the NTAA gradually decreases to minimal values in the NK3B and the CC3b-CC4a subzones transition.

In this study, only the taxa that presented significant variations in all studied successions are considered (Figs. 4-6). Thereby, the following groups are not described: other *Watznaueria* species (*W. biporta* and *W. britannica*), *A. infracretacea*, *D. ignotus*, and *R. crenulatus*. For Zalidou and Aït Hamouch sections, the absolute abundance (AA, nannofossils/gram of rock) of

494 nannofossil taxa are shown in Figs. Supp. 2 and 3, respectively (see also Supplementary Table).
495 The average accumulation rate (AR, nannofossils/m^2/year) of each considered nannofossil
496 taxon is generally higher at Zalidou (Fig. 4) compared to Aït Hamouch (Fig. 5), except for
497 nannoconids their average AR is higher at Aït Hamouch than at Zalidou (Supplementary Table).
498 The AR of nannofossil taxa in the onshore sections generally decreases during the *B.*
499 *campylotoxus* LSz and *K. inostranzewi* StZ (NK3A and lower CC3b subzones), earlier than the
500 decrease of NTAR. Their AA in Hole 416A decreases during the same calcareous nannofossil
501 subzones. Notably, the reductions in the NTAR and the AR of taxa are observed earlier in Aït
502 Hamouch (*B. campylotoxus* LSz) with respect to Zalidou (*K. inostranzewi* StZ). During the rest
503 of the successions, the AR or AA of nannofossil taxa generally follow the same trend as that of
504 the NTAR or NTAA, respectively (Figs 4-6).
505 **4.3.2 Calcareous nannofossil diversity indices and relative abundances**
506 Taxa richness and equitability are plotted for Zalidou (Fig. 4), Aït Hamouch (Fig. 5),
507 and Hole 416A (Fig. 6). The offshore succession is characterized by higher nannofossil
508 diversity indices compared to those of the onshore sections. At Zalidou (Fig. 4), the taxa
509 richness shows a long-trend decrease from the early to late Valanginian. The equitability is
510 highest in the early Valanginian. At Aït Hamouch (Fig. 5), the taxa richness decreases to lowest
511 values in the late early Valanginian and in the early late Valanginian. The lowest equitability
512 values are recorded in the late early Valanginian. At Hole 416A (Fig. 6), both taxa richness and
513 equitability increase during the lower NK3A and CC3a to lower CC3b subzones. Upwards, the
514 equitability remains high in the rest of the Valanginian, whereas the richness decreases.
515 At Zalidou (Fig. 4), the RA of *W. barnesiae/fossacincta* is high in the early Valanginian
516 and around the early-late Valanginian transition, then it decreases during the early late
517 Valanginian. At Aït Hamouch (Fig. 5), its RA increases during the late early Valanginian and
518 during the late Valanginian. The RA of *D. lehmanii/subbeticus* increases at Zalidou in the late

519 Valanginian and remains high upsection. Whereas, its RA at Aït Hamouch decreases in the late
520 early Valanginian, followed by a re-increase in the early late Valanginian. In both onshore
521 sections, the RA of small *Zeugrhabdotus* spp. increases to highest values in the late
522 Valanginian. The RA of *B. ellipticum* decreases in both onshore sections to minimal values
523 from the late early Valanginian. Its RA re-increases only at Aït Hamouch in the late
524 Valanginian. The RA of nannoconids declines to minimal values in Zalidou (Fig. 4) from the
525 late early Valanginian to the early late Valanginian. Whereas, at Aït Hamouch (Fig. 5), the RA
526 of nannoconids is low in the early Valanginian and increases to maximal values in the early late
527 Valanginian. Change in the proportion of narrow-canal nannoconids within nannoconid
528 population is observed at Aït Hamouch. Their proportion is high from the early Valanginian to
529 the early late Valanginian compared with the rest of the Valanginian (Fig. 5).

530 At Hole 416A (Fig. 6), the RA of *W. barnesiae/fossacincta* increases during the upper
531 NK3A and CC3b subzones. The RA of *D. lehmanii/subbeticus* is relatively stable throughout
532 the Valanginian. The RA of small *Zeugrhabdotus* spp. increases during the upper NK3A and
533 CC3b subzones. The RA of *B. ellipticum* decreases during the same biozones. The RA of
534 nannoconids decreases in the upper NK3A to NK3B and upper CC3b to CC4a subzones. The
535 proportion of narrow-canal nannoconids within the nannoconid population is generally lower
536 in the lower NK3A and CC3a subzones compared with the rest of the succession.

537 **4.4 Calcium carbonate content and carbon isotopes**

538 The $CaCO_3$ (%) contents range between 15 – 93 (avg. 49 %) at Zalidou, 14 – 88 (avg.
539 41 %) at Aït Hamouch, and 4 – 92 (avg. 23 %) at Hole 416A. At both onshore sections (Figs.
540 4-5), the highest $CaCO_3$ content is recorded in the early Valanginian. At Zalidou, the decrease
541 in $CaCO_3$ content is concomitant with a lithological change to more clastic-rich marlstone-
542 limestone beds. At Hole 416A (Fig. 6), the $CaCO_3$ content decreases and exhibits fewer

fluctuations in the upper NK3A to NK3B and upper CC3b to CC4a subzones, compared with down-section.

The $\delta^{13}C_{carb}$ values range between –2.8 and +1 (avg. –0.8 ‰) at Zalidou, –3.3 and +0.4 (avg. –1.5 ‰) at Aït Hamouch, and between –4.9 and +1.9 (avg. –1.0 ‰) at Hole 416A. At Zalidou (Fig. 4), the $\delta^{13}C_{carb}$ increases from –2.4 ‰ to +1 ‰ between the latest early Valanginian (*K. inostranzewi* StZ, upper NK3A, and upper CC3b subzones) and the latest Valanginian (upper *O. nicklesi* StSz, upper NK3B, and upper CC4a subzones). At Aït Hamouch (Fig. 5), the $\delta^{13}C_{carb}$ increases from ~ –2.5 ‰ to ~ –0.4 ‰ between the latest early Valanginian (*K. inostranzewi* StZ, upper NK3A, and upper CC3b subzones) and the early late Valanginian (lower *N. peregrinus* StZ, upper NK3A, and lower CC4a subzones). Accordingly, the carbon-isotope positive shift is of magnitude 3.7 ‰ and 2.3 ‰ at Zalidou and Aït Hamouch, respectively. Then, the $\delta^{13}C_{carb}$ smoothly decreases in the rest of the late Valanginian in both, Zalidou (~ +0.1 ‰) and Aït Hamouch (~ –1.1 ‰). At Hole 416A, the $\delta^{13}C_{carb}$ does not show any positive shift (Fig. 6).

5. Interpretation

5.1 Sedimentary paleoenvironment

Except in the lower Valanginian condensed strata of the Obbay section, we did not observe oolites in the limestone beds. This indicates a rather low energy depositional environment in the EAB during most of the Valanginian. As a matter of fact, since trade winds blew to the west, and because the EAB is located on the western coast of Africa, it was little affected by intense tropical storms. These storms may have been generated in the Atlantic Ocean, but were pushed to the west by the trade winds and to the north by the Coriolis force (see Trabucho-Alexandre et al., 2011; Pohl et al., 2019; Jaillard et al., 2021). Therefore, the EAB can be considered to have been a low energy ramp gently sloping toward the ocean. However, the numerous oolites observed on the Obbay swell (Fig. 3) indicate that the

shallowest part of the water column was moderately agitated, at least in the early Valanginian. Actually, in the sandstone and sandy limestone beds of late early and late Valanginian age, ripples and scarce trough cross beds indicate a moderate wave activity, while planar parallel laminations suggest tidal processes. Also, the occurrence of thin-bedded HCS in shallow marine beds suggests the occurrence of storms of low intensity. During the late early Valanginian and late Valanginian, the moderate hydrodynamic activity of the surficial part of the water column also accounted for the occurrence of sandstone or sandy limestone beds above the surfaces interpreted as sequence boundaries (Fig. 3). This may be due to the erosion occurring during low sea-level periods, which removed the shale particles and cleared up quartz grains from the sediments. The quartz grains were then deposited as sandy beds during the subsequent transgression.

The scarcity of corals and algae, the abundance of agglutinated foraminifers, and the presence of bryozoans in the calcareous beds (mainly early Valanginian) suggest temperate to cold sea water temperatures. Because of the activity of trade winds, the EAB was probably subjected to upwellings (Price et al., 1995; Poulsen et al., 1998). Oceanic upwellings may explain both the cold to temperate waters, and the common occurrence of phosphate in shallow deposited beds.

The abundance of ostreids and plicatulids throughout the section suggests mesotrophic conditions, while the presence of agglutinated foraminifers in the early Valanginian suggests, additionally, an oxygen depletion at that time (e.g., Kuhnt et al., 1996; Reolid et al., 2008; Kender and Kaminski, 2017). This interpretation is supported by the abundance of pyrite in the lower Valanginian marlstone of the southern sections. Oxygen depletion, however, must have been mild or sporadic since echinoids are common at that time. Mesotrophic conditions were most likely related to the terrigenous influx of fine-grained clastic particles, more abundant toward the north and east (Fig. 9). This is supported by the sporadic occurrence of wood and

leaf fragments (Zalidou) in Valanginian deposits. Actually, a combination of high terrigenous supply, temperate to cold temperature, and the presence of upwellings favors the development of heterozoan carbonate systems (Michel et al., 2018).

5.2 Paleogeography

In the early Valanginian, the northern sections were marked by open marine, oyster-rich shallow carbonate shelf facies exhibiting several karstified surfaces. Whereas, the southern ones presented distal facies marked by thick marlstone intervals, abundant cephalopods, and the lack of emergence evidence (Fig. 9). During the late Valanginian, the northern sections recorded the progradation of a clastic sedimentary system (Fig. 9), which indicates that the clastic supply proceeded from the Central High Atlas (Ferry et al., 2007). Clastic supply was interrupted by a significant erosion period (D7, Figs. 3, 9), likely related to an emergence episode. Furthermore, the uppermost Valanginian deposits end up with foreshore deposits and are capped by an emergence surface to the northeast (Ida w Iddar). Conversely, the coeval sediments in Zalidou bear cephalopods and plicatulids, and end up with a submarine erosional surface to the southwest (Aït Hamouch). The south-westward sloping topography is supported by the onlap of the lower upper Valanginian sequence to the north or northeast (Fig. 3). Although sandstone prograded in the northern part of the basin during the late Valanginian, the southernmost section (Aït Hamouch) displays sandy layers in the late early to earliest late Valanginian (Fig. 9). This suggests that the course of rivers that supplied quartz grains to the EAB was changing through time.

In the Obbay section, the lower Valanginian succession is very condensed (Fig. 3). Two explanations may be proposed. First, the presence of strong upwelling currents in the early Valanginian (Price et al., 1995; Poulsen et al., 1998) could have accounted both for the condensation and the abundance of phosphate and glauconite (Föllmi, 1996; Puhfal and Groat, 2017). Second, incipient movements of the Amsittene diapir (e.g., Tari and Jabour, 2013) or

compressional tectonics in Early Cretaceous times (Bertotti et al., 2012; Fernández-Blanco et al., 2020) may have locally uplifted this area. If so, the area became a shallow swell reaching the Fair-Weather Wave Base, on which a high energy regime caused condensation. A combination of both upwelling and uplift is likely. The fact that condensation disappears during the late Valanginian sea level rise suggests that either, upwelling currents were less active, or more probably, their activity was distributed and mitigated in the thicker water column.

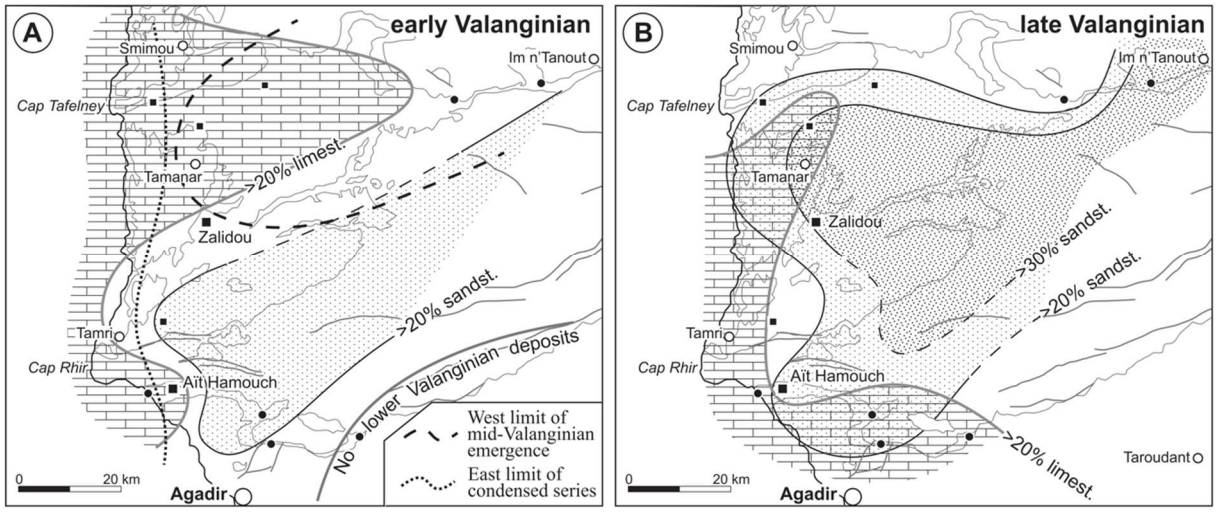

Fig. 9. Paleogeographic sketch of the Essaouira-Agadir Basin showing the distribution of sandstone and limestone in the (A) lower Valanginian and the (B) upper Valanginian deposits. Reconstruction based on data from this study (black squares) and from Ferry et al. (2007) (black dots).

5.3 Preservation of a calcareous nannofossil primary signal

The relative abundance (RA) of the solution-resistant *W. barnesiae/fossacincta* taxa is used as an indication of the preservation state. Roth and Krumbach (1986) suggested that relative abundances of *W. barnesiae* > 40 % indicate high degree of diagenesis and dissolution, while Williams and Bralower (1995) suggested that even higher proportions (> 70 %) indicate assemblage alteration. In the studied samples, the RA of *W. barnesiae/fossacincta* is on average 41 % at Zalidou, 43 % at Aït Hamouch, and 37 % at Hole 416A. Additionally, RA ranges of *W. barnesiae/fossacincta* in this study are not very different from those recorded in other basins: ~50 – 90 % in Lombardian and Belluno Basins-northern Italy (Erba and Tremolada, 2004); 48 – 78 % in the Vocontian Basin, SE France (Reboulet et al., 2003); 18 – 77 % in DSDP Site 535,

639 Gulf of Mexico (Kessels et al., 2006); and 22 – 59 % in DSDP Hole 603B, northern Atlantic
640 (Bornemann and Mutterlose, 2008). Also, *W. barnesiae/fossacincta* dominate the assemblage
641 in the Subbetic Domain (SE Spain) although no quantification was done (Aguado et al., 2018).
642 Most of these studies come from sections having experienced low levels of diagenesis,
643 supporting that the dominance of *W. barnesiae/fossacincta* is not a local effect.

644 The correlation between the RA of *W. barnesiae/fossacincta* and the taxa richness was
645 tested in all the studied successions (Fig. 8). Despite the fact that a negative correlation can be
646 suspected (r = –0.37, $p_{uncorr.}$= 0.0005, n= 85 in Zalidou; r= –0.45, p_{uncorr}= 0.0006 , n= 54 in Aït
647 Hamouch; and r= –0.41, p_{uncorr}= 0.005, n= 44 in Hole 416A), the preservation classes show that
648 samples with strong dissolution and recrystallization do not necessarily correspond to high
649 proportions of *W. barnesiae/fossacinta* (Fig. 8). These samples are homogenously distributed
650 for any given proportion of *W. barnesiae/fossacinta*. Moreover, some samples with good and
651 moderate preservation present a high percentage (> 40 %) of *W. barnesiae/fossacincta*, which
652 implies that the high proportions of *W. barnesiae/fossacincta* can also be part of the original
653 calcareous nannofossil assemblage during the Valanginian.

654 Thereby, based on all aforementioned evidence, we assume that the nannofossil
655 assemblages of both the Essaouira-Agadir Basin and the DSDP Hole 416A are slightly affected
656 by diagenetic alteration but still hold a primary signal that can be used for the paleoceanographic
657 reconstruction.

658 **5.4 Time succession in calcareous nannofossil assemblages**

659 The nannofossil total accumulation rate (NTAR) and nannofossil total absolute
660 abundances (NTAA) along with the accumulation rate (AR), absolute abundance (AA), and
661 relative abundance (RA) of the major calcareous nannofossil taxa demonstrate variations from
662 the early to late Valanginian. This, associated with the sedimentology results, will allow the
663 reconstruction of the paleoceanographic conditions on the central Moroccan margin and to

664 better constrain the evolution of paleoceanographic conditions around the Weissert Event. As
665 the late Berriasian *p.p.* was only recognized at Zalidou and the early Hauterivian *p.p.* was only
666 recognized at Aït Hamouch, the discussion will be focused on paleoceanographic conditions
667 during the Valanginian.

668 For the paleoceanographic reconstruction, the NTAR (and NTAA for Hole 416A) is
669 used as a proxy to estimate the nannofossil production. The accumulation rates and abundances
670 (absolute and relative) of the selected nannofossil taxa are used as a proxy for surface-water
671 fertility levels. The ecological affinity of calcareous nannofossil taxa used for this purpose,
672 along with the associated literature, are summarized in Table 1.

673 Table 1. Main ecological affinity of the calcareous nannofossil taxa used for paleoceanographic
674 reconstruction, following the specified literature. 1. Bersezio et al. (2002); 2. Bornemann et al.
675 (2003); 3. Coccioni et al. (1992); 4. Crux (1989); 5. Erba (1992); 6. Erba et al. (1992); 7. Erba
676 (1994); 8. Eleson and Bralower (2005); 9. Giraud et al. (2003); 10. Herrle (2002); 11. Herrle et
677 al. (2003); 12. Lees (2002); 13. Lees et al. (2005); 14. Mattioli et al. (2014); 15. Mutterlose
678 (1991); 16. Mutterlose (1992a); 17. Mutterlose (1992b); 18. Mutterlose and Kessels (2000); 19.
679 Mutterlose et al. (2003); 20. Mutterlose et al. (2005); 21. Noël et al. (1987); 22. Pauly et al.
680 (2012); 23. Pittet and Mattioli (2002); 24. Premoli Silvá et al. (1989); 25. Roth (1981); 26. Roth
681 (1989); 27. Roth and Bowdler (1981); 28. Roth and Krumbach (1986); 29. Street and Bown
682 (2000); 30. Thierstein (1980); 31. Tremolada et al. (2006); 32. Watkins (1989); 33. Williams
683 and Bralower (1995).

Taxa	Fertility of surface waters	Ecological strategy	Paleoceanography
B. constans	eutrophic[5, 18, 19, 24, 25, 26, 27, 28, 29, 32, 33]	low diversified assemblages[18]	upwelling[5, 18, 24, 25, 26, 27, 28]
	meso-eutrophic[8]	eurytopic[17]	shelf surface-waters[21, 29]
B. ellipticum	eutrophic[9, 27] meso-eutrophic[16]	r-selected[18]	upwelling[6, 12, 30]
D. lehmanii	eutrophic[1, 4, 14, 20, 31, 33]		transgressive intervals[4] upwelling[33]
D. subbeticus	eutrophic[14]		distal environments[14]
nannoconids	oligotrophic[1, 2, 3, 7, 11, 18] meso-oligotrophic[22]	r-selected[29]	neritic[10, 25, 27, 28, 29] lower photic zone[2, 7]
W. barnesiae	oligotrophic[8, 10, 11, 26, 28, 30, 31, 32] mesotrophic[23] eurytrophic[14]	eurytopic[13, 15, 21, 29] r-selected[12, 23, 30]	oceanic setting[27]
W. barnesiae/fossacincta		eurytopic[13]	
Z. erectus	eutrophic[5, 9, 10, 11, 24, 25, 26, 27, 28, 29, 32, 33]	r-selected[6, 12, 23]	upwelling[5, 24, 25, 26, 27, 28]
	more eutrophic than *B. constans*[6]	low diversified assemblages[18]	shelf-surface water[18]
Small *Zeugrhabdotus* spp.	eutrophic[6, 32]		

684 *B. ellipticum* is considered as a morphotype of *B. constans* (Bornemann and Mutterlose, 2006)

685 **5.4.1 The Zalidou section**

686 During the early Valanginian (*N. premolicus* StSz to upper *B. campylotoxus* LSz, NK3A
687 and upper CC3a to lower CC3b calcareous nannofossil subzones), except for small fluctuations
688 the nannofossil production did not vary and was relatively high (Fig. 4). During the *N.*
689 *premolicus* StSz and *N. subtenuis* LSz (lower NK3A and CC3a to lower CC3b subzones),
690 favorable surface-water conditions allowed the development of the nannofossil community as
691 suggested by the highest diversity indices. Additionally, local mesotrophic conditions are
692 suggested by the abundant high-fertility taxa. Afterwards, a decoupling between NTAR,
693 diversity indices, AR, and RA of the selected taxa is recorded. In the *B. campylotoxus* LSz
694 (within the NK3A and CC3b subzones), surface-water conditions became less favorable,
695 leading to a decrease in the AR of all nannofossil taxa and in the diversity. Only the eurytopic
696 *W. barnesiae/fossacincta* remained high during this time interval, and the nannofossil
697 production was maintained (Fig. 4).

698 In the latest early Valanginian (*K. inostranzewi* StZ, upper NK3A and upper CC3b
699 subzones), the nannofossil production collapsed as supported by both, minimal NTAR and
700 minimal AR of all nannofossil taxa (Fig. 4). Excluding poor preservation, this collapse could
701 be explained by major paleoenvironmental changes.

702 Afterwards, in the late Valanginian (*S. verrucosum* to upper *O. nicklesi* StSz, upper
703 NK3A to NK3B and uppermost CC3b to lower CC4a subzones), the nannofossil production
704 gradually increased, supported by the re-increasing NTAR and AR of all nannofossil taxa (Fig.
705 4). The end of this recovery phase was marked by a high nannofossil production and meso-
706 eutrophic conditions. The meso-eutrophic conditions are interpreted from the important
707 increase in the small *Zeugrhabdotus* spp. during the late Valanginian (upper *N. peregrinus* and
708 upper *O. nicklesi* StSz, NK3B and CC4a subzones). This time interval was also characterized
709 by the recovery of nannoconids (Fig. 4).

Lastly, in the remaining late Valanginian, the nannofossil production slightly decreased with similar magnitudes as those observed in the early Valanginian. However, despite a decrease in surface-water fertility, the fertility remained higher with respect to the early Valanginian as supported by the higher RA of the small *Zeugrhabdotus* spp. (Fig. 4).

5.4.2 The Aït Hamouch section

During the early Valanginian (*N. premolicus* StSz to *N. subtenuis* LSz, lower NK3A and CC3a to lowermost CC3b calcareous nannofossil subzones), the nannofossil production was high with values higher compared to the Zalidou section (Figs. 4, 5). A decoupling between NTAR, diversity indices, AR, and RA of the selected nannofossil taxa is also observed (Fig. 5). During the *N. premolicus* StSz (lower NK3A and CC3a subzones), mesotrophic conditions in surface waters and a thick photic zone allowed a diverse calcareous nannofossil community to flourish. Also, these conditions allowed the development of benthic carbonate producers, such as agglutinated foraminifers, ostreids, and plicatulids (see section 4.1). Afterwards, during the *N. subtenuis* LSz, the surface-water conditions became less favorable for both high-fertility taxa and nannoconids. As at Zalidou, the eurytopic *W. barnesiae/fossacincta* remained high during this time interval and nannofossil production was maintained (Fig. 5).

During the late early Valanginian (*B. campylotoxus* LSz to *K. inostranzewi* StZ, NK3A and CC3b subzones), the nannofossil production gradually declined and collapsed (Fig. 5). Excluding poor preservation, the trigger of the collapse can be also explained by major paleoenvironmental changes. Decline in the nannofossil production is suggested from the drastic decrease in accumulation rate and abundance of the dominant taxa, *W. barnesiae/fossacincta*. Nannofossil production remained low during the early late Valanginian (lower *N. peregrinus* StZ, upper NK3A Subzone and CC3a-CC3b subzones transition; Fig. 5). Decreasing percentages of *W. barnesiae/fossacincta* within the nannofossil assemblage explain

734 that all other taxa show increasing percentages (in particular nannoconids) despite decreasing
735 AR.

736 Afterwards, in the late Valanginian (upper *N. peregrinus* to *C. furcillata* StZ, upper
737 NK3A to NC4A and CC4a subzones), the nannofossil production first recovered before
738 reaching higher magnitudes than that of the early Valanginian (Fig. 5). This is attested by the
739 increasing NTAR, and AR of all taxa. In parallel, enhanced surface-water trophic levels are
740 demonstrated by the increasing abundances of both *D. lehmanii/subbeticus* and small
741 *Zeugrhabdotus* spp.. The nannoconid AR is maximal, and is associated with decreasing
742 proportion of narrow-canal forms (Fig. 5). Lastly, in the latest Valanginian (*T. callidiscum* StSz,
743 uppermost NC4A and CC4a subzones), the nannofossil production and trophic levels decreased
744 to magnitudes slightly lower than that of the early Valanginian.

745 **5.4.3 DSDP Hole 416A**

746 The lower NK3A and CC3a calcareous nannofossil subzones are characterized by an
747 increase in the nannofossil production, as suggested by both increasing NTAA and abundances
748 of meso-eutrophic taxa (Fig. 6). Marine conditions were also favorable for the development of
749 nannoconids, as their absolute abundance is higher compared with both onshore sections (Fig.
750 6, and Figs. Supp. 2-3). In addition, the nannoconids were mainly represented by narrow-canal
751 forms with the large dominance of *N. steinmannii* (Fig. 6). The assumption that narrow-canal
752 *Nannoconus* inhabited the deep photic zone under stratified waters and a deep nutricline (Erba,
753 2004, 1994) has been challenged by Mattioli et al. (2014), who showed that *N. steinmannii*
754 could have affinity for destratified surface waters. Hole 416A is characterized by turbiditic
755 sequences and low calcium carbonate contents within the Valanginian sediments. The repeated
756 input of clastic material would prevent the stratification of the water column.

757 Upsection, in the upper NK3A-NK3B and CC3b-CC4a subzones, the NTAA and AA
758 of all taxa decrease (Fig. 6). Reduced surface-water fertility during this time interval is shown

by the decreasing relative abundance of high-fertility taxa. Nannoconids decline slightly after the fertility decreased in the uppermost NK3A and upper CC3b subzones. These are interpreted as unfavorable surface-water conditions, similar to those observed in the onshore Essaouira-Agadir Basin.

The onset of the nannofossil production recovery, similar to that of NTAR observed onshore, seems to occur in the topmost samples (Fig. 6). However, the recovery phase itself as recorded in the onshore settings seems to be missing at Hole 416A.

5.5 The carbon isotope record and identifying the Weissert Event

At Zalidou, we identify the Weissert Event from the base of the carbon-isotope (CI) positive shift (16.25 m) until the climax (32.8 m; Fig. 10), following the formal definition of Erba et al. (2004). The CI positive shift is observed from the lower part of the *K. inostranzewi* StZ to the upper part of the *O. nicklesi* StSz (upper NK3A to upper NK3B and upper CC3b to upper CC4a calcareous nannofossil subzones). The top of the Weissert Event is recorded just below the LO of the nannofossil biomarker *T. verenae*.

At Aït Hamouch, the *S. verrucosum* StZ and the *O. nicklesi* StSz are not recognized (see section 2.1). Additionally, the *N. peregrinus* StZ is reduced (~7 m) compared with Zalidou (~14 m). This can be also observed from the reduced NK3B calcareous nannofossil Subzone in Aït Hamouch (1.5 m) compared with Zalidou (12.5 m; Fig. 10). Moreover, the smooth increase in $\delta^{13}C_{carb}$ within the CI positive shift is suspected to be missing from Aït Hamouch. This phase is observed during the *O. nicklesi* StSz in Zalidou (Fig. 10). Thereby, considering both the biostratigraphy of ammonites and calcareous nannofossils along with the chemostratigraphy from carbon-isotope analysis, it is highly possible that part of the late Valanginian could be missing from Aït Hamouch. Furthermore, the paleoceanographic reconstruction from calcareous nannofossils at Zalidou showed a collapse in nannofossil production just after the onset of the identified Weissert Event interval (*K. inostranzewi* StZ; Fig. 10). The collapse was

784 followed by an increase in both nannofossil production and surface-water fertility, and then by
785 slightly decreasing nannofossil production and fertility during the rest of the Weissert Event
786 interval. Using all the above-mentioned information, the Weissert Event interval at Aït
787 Hamouch is cautiously identified from 32.2 to 39.2 m (Fig. 10). This identified Weissert Event
788 interval starts just before the nannofossil production collapse, and terminates when both
789 nannofossil production and surface-water fertility recover and prior to the LO of *T. verenae*.
790 The LO of *T. verenae* demonstrates that it is a reliable event.

791 At Hole 416A, the measured $\delta^{13}C_{carb}$ values do not show any positive shift (Fig. 6).
792 Wortmann and Weissert (2000) measured $\delta^{13}C_{org}$ in samples from Hole 416A and identified a
793 $\delta^{13}C_{org}$ positive excursion from –1420 to –1300 mbsf, which is not recognized in this study (Fig.
794 6). In both onshore sections, the base of the Weissert Event is roughly near to the FO of *H.*
795 *circumradiatus*, although we acknowledge its occurrence is very sporadic. Therefore, we
796 tentatively consider the interval corresponding to the Weissert Event from –1303 to –1122 mbsf
797 in Hole 416A (Fig. 10). Its base is after the onset of the decline in nannofossil production and
798 surface-water fertility, similar to the observation from the onshore sections. The explanation
799 for the absence of a CI positive shift at Hole 416A is unclear. The supposed positive shift might
800 have been diluted by the highly reworked material and terrigenous supply, or concealed by the
801 graded turbidite cycles and/or by the high sedimentation rates known for this interval (Lancelot
802 et al., 1980; Schlager, 1980). Indeed, the Valanginian sediments at Hole 416A are more than
803 400 m thick (Lancelot et al., 1980). Furthermore, the carbonate sediments in all studied
804 successions, including Hole 416A, generally present a similar order of magnitude to the $\delta^{13}C_{carb}$
805 values (~ –1.0 ‰).

806 In the Essaouira-Agadir Basin (EAB), the calibration of the Weissert Event with
807 calcareous nannofossils allows the assignment of the CI positive shift to the upper NK3A-upper
808 NK3B subzones (upper CC3b to “middle” CC4a). The base of the Event is close to the FO of

809 *H. circumradiatus*, whereas its end coincides roughly with the LO of *T. verenae* (Fig. 10). The
810 Zalidou section is the most appropriate section to study the Weissert Event in the EAB.
811 Although sedimentological discontinuities and related hiatuses are present, it is the most
812 complete section and well dated by ammonite and nannofossil biostratigraphy (Fig. 10). The
813 $\delta^{13}C_{carb}$ clearly shows a carbon-isotope positive shift similar to that observed elsewhere.

814 **5.6 Basin-wide paleoceanographic reconstruction**

815 In the EAB, a high calcareous nannofossil production and mesotrophic surface-water
816 conditions occurred in the early Valanginian before the Weissert Event interval. This time-
817 interval was also characterized by a low energy depositional environment and a mild oxygen-
818 depletion (see section 5.1), which could infer stratification of the water-column. However, some
819 differences existed between the different settings due to their respective paleogeographic
820 location (Fig. 9). The nannofossil production was higher at Aït Hamouch with respect to
821 Zalidou in the early Valanginian (Fig. 10). Aït Hamouch was more distal from the shoreline
822 with respect to Zalidou (see section 5.2; Fig. 9). Consequently, the greater depth of deposition
823 at Aït Hamouch and its location farther from the coastline allowed the development of a large
824 and diverse nannofossil community in a thicker photic zone. Also, trophic levels in surface
825 waters were higher at Aït Hamouch than at Zalidou (Fig. 10). Nutrient input in the EAB was
826 generally maintained from both, clastic river input and oceanic upwelling (see sections 5.1 and
827 5.2). During the early Valanginian, the northern part of the EAB (Zalidou section) was less
828 influenced by clastic river influx with respect to the southern part (Aït Hamouch; see Fig. 9).
829 Moreover, Aït Hamouch was potentially fed by nutrients from the nearby upwelling system
830 observed in the Obbay section. Although, the highest nannofossil production was in Hole 416A,
831 being offshore with the thickest photic zone (Fig. 6, and Figs. Supp. 2-3). Fertility levels
832 decreased prior to the Weissert Event interval in the late early Valanginian in all successions
833 (Fig. 10). Nonetheless, a high nannofossil production was maintained by the eurytopic *W.*

834 *barnesiae/fossacincta*. The fertility decrease was probably related to a major sea level fall
835 recorded on the central Moroccan margin, and culminated with the expression of the D4 and
836 D5 sedimentary discontinuities (Figs. 3, 10). The sea level fall first impacted the nannofossil
837 community of the distal Aït Hamouch section with the possible ocean-ward migration of the
838 upwelling system away from this site, which should have consequently reduced nutrient input.
839 At the same time, storm deposits and coarse clastic input are recorded at Aït Hamouch (section
840 5.1). Additionally, more turbid surface-water due to riverine-clastic input must have favored
841 the proliferation of the eurytopic *W. barnesiae/fossacincta*. Afterwards, the entire nannofossil
842 community collapsed at the onset of the Weissert Event and in its lower part, around the early-
843 late Valanginian transition (Fig. 10). Offshore, in Hole 416A, the onset of the surface-water
844 fertility decline (upper NK3A and CC3b subzones) and the later collapse of the nannofossil
845 community (NK3B and CC3b-CC4a subzones) seem to have occurred slightly later than in the
846 EAB (Fig. 10). We similarly relate these changes to the maximum drop of sea level expressed
847 by the D4 and D5 discontinuities in the EAB. The collapse is observed later in the distal Hole
848 416A possibly due to the hiatuses related to emergences observed on the platform which are
849 not recorded in a deep setting. The nannofossil production gradually recovered during the
850 Weissert Event in the early late Valanginian and was associated with a rising sea-level (section
851 4.1, Fig. 10). Higher riverine clastic input is recorded in the north (Zalidou) with respect to the
852 south (Aït Hamouch; see Fig. 9). High input of clastics and associated nutrients could explain
853 the early recovery at Zalidou in the nannofossil production and in the abundance of high fertility
854 taxa. At Aït Hamouch, the recovery occurred later, and can be explained by the nutrient input
855 that started arriving from the upwelling system. Maximal nannofossil production along with
856 eutrophic surface-waters are recorded only at Zalidou during the upper part of the Weissert
857 Event interval in the late Valanginian (upper *N. peregrinus* to upper *O. nicklesi* ammonite StSz,
858 NK3B and lower CC4a subzones; Fig. 10). Eutrophic surface-waters occurred during maximal

flooding and continuous continental influx (section 5.1, Fig. 10). Lastly, a decrease in both the nannofossil production and surface-water fertility occurred after the Weissert Event interval in the rest of the late Valanginian (Fig. 10). Although, trophic levels were higher compared with the early Valanginian. An abrupt increase in the nannofossil production and surface water fertility is observed only at Aït Hamouch during the late Valanginian (*C. furcillata* StZ, NC4A and upper CC4a subzones) after the Weissert Event. At this time, the depositional environment in Aït Hamouch corresponded to an outer shelf (Fig. 9), possibly with a thick photic zone for the nannofossils to flourish. Whereas, the depositional environment in Zalidou corresponded to a clastic shelf with higher turbidity responsible for a reduced photic zone.

The nannoconids in the EAB and Hole 416A, mainly represented by *N. steinmannii* (narrow-canal form), generally show a distal-to-proximal gradient with highest abundances in Hole 416A followed by Aït Hamouch and Zalidou, successively. Also, the nannoconids were "thriving" during periods of relatively high fertility in surface-waters in all studied successions (Fig. 10). Initially, this is observed in the early Valanginian onshore (*N. premolicus* StSz to lowermost *N. subtenuis* StSz in Aït Hamouch and *N. subtenuis* LSz in Zalidou section, lower NK3A and CC3a subzones) and in the lower part of the Valanginian interval offshore. Then, a nannoconid decline is recorded onshore in the early Valanginian (*N. neocomiensiformis* to lower *N. peregrinus* StZ, NK3A to lower NK3B subzones, CC3b to lower CC4a subzones), earlier in the southernmost section Aït Hamouch (Fig. 10). Offshore, in Hole 416A, the decline occurred slightly later in the uppermost NK3A to lower NK3B and upper CC3b to lower CC4a subzones. On the central Moroccan margin, this decline can be explained by the drop of sea-level that negatively impacted the entire nannofossil community. A fall of sea-level reduces the size of the photic zone (thickness and geographic extent), and can thus explain the observed decrease within the nannoconid population. DSDP Hole 416A was impacted later due to its distal setting and thicker photic zone. Afterwards, the nannoconids recovered in the late

884 Valanginian (upper *N. peregrinus* StZ, NK3A-NK3B and lower CC4a subzones) during the
885 Weissert Event interval. The nannoconids recovery occurred during periods of relatively high
886 surface-water fertility in all studied successions (Fig. 10). These time-intervals were
887 characterized by a high sea-level, which allowed the development of a thicker photic-zone and
888 consequently various habitats to be occupied. Moreover, during the late early and late
889 Valanginian, the occurrence of thin-bedded HCS restricted to shallow marine beds suggests the
890 occurrence of storms of low intensity (section 5.1). This could suggest the absence of
891 stratification in the water-column.

892 Different positions within the photic zone were proposed for narrow- and wide-canal
893 *Nannoconus* (Table 1). At Aït Hamouch, the proportion of narrow-canal forms (mainly *N.*
894 *steinmannii*) within the nannoconid population reached its highest value during the sea-level
895 fall interval and coincided with maximum clastic input (Fig. 5). Afterwards, although the clastic
896 input was reduced, the proportion of narrow-canal forms within the nannoconid population
897 decreased all along the succession. Then, as shown for Hole 416A, high abundance of *N.*
898 *steinmannii* was not associated with a stratified water column but occurred during high clastic
899 input (see section 5.4.3). This implies a shallow nutricline. Our results confirm the assumption
900 of Mattioli et al. (2014) suggesting that *N. steinmannii* inhabited de-stratified surface waters.

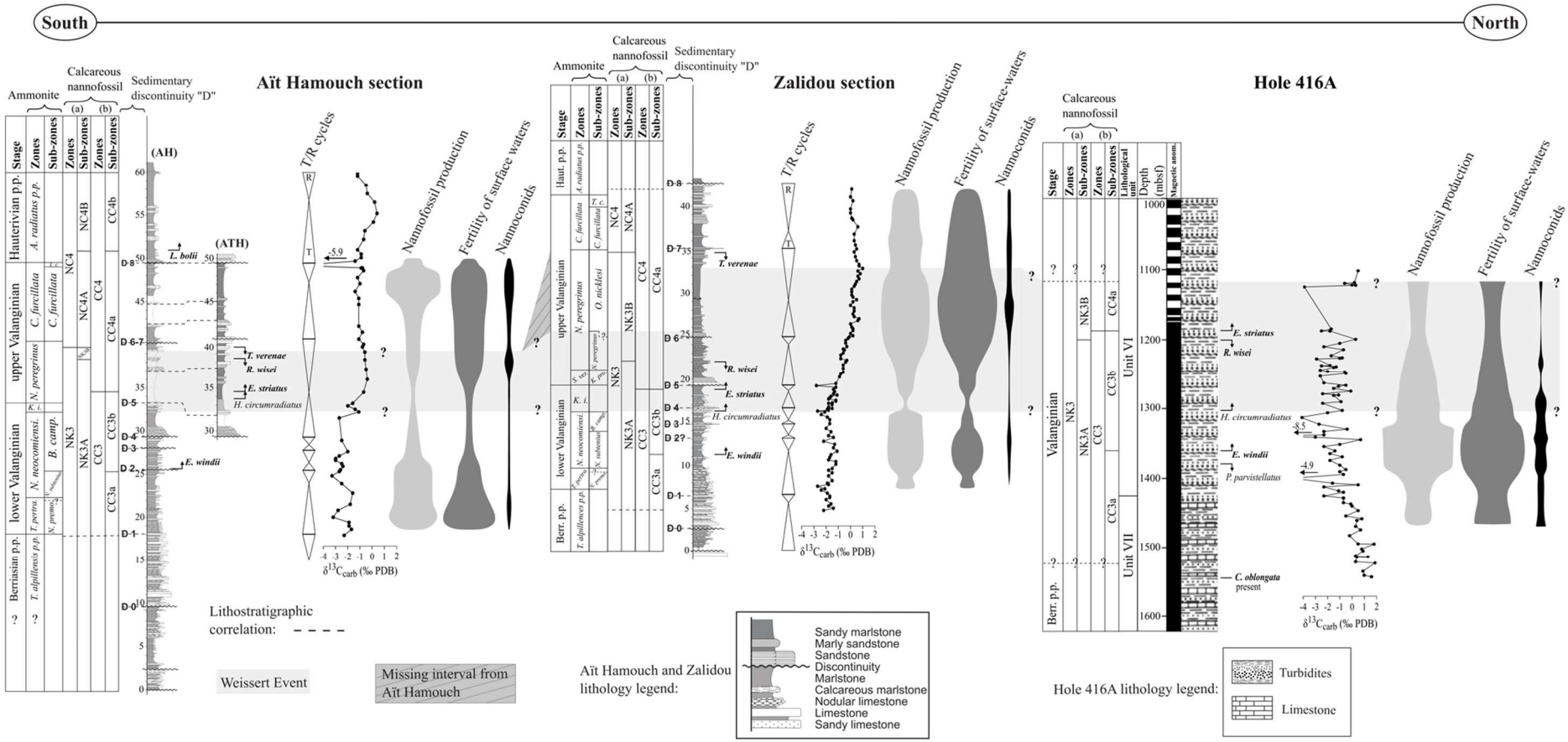

Fig. 10. Synthesis of the paleoceanographic conditions on the central Moroccan margin. Gray shading refers to the Weissert Event interval, for more details see section 5.5. Striped-correlation refers to a possible missing interval in Aït Hamouch (section 5.5). Simplified schemes of nannofossil production, fertility, and nannoconids abundance are comparable between Zalidou and Aït Hamouch since they are based on the accumulation rate results. Whereas, those of Hole 416A are based on the absolute abundance results. Also added are the transgression (T) – regression (R) cycles (sections 5.1 and 5.2).

907 **5.7 Integrating the central Moroccan margin in a global paleoceanographic**
908 **reconstruction**

909 In order to globally reconstruct the fertility in surface-waters during the Weissert Event,
910 the paleoceanographic conditions (reconstructed from calcareous nannofossil data) of the
911 central Moroccan margin are compared with those of other basins. All of the considered studies
912 used the following taxa (small *Zeugrhabdotus* spp., *B. ellipticum*, *D. ignotus*, and *D. lehmanii*)
913 as indicators of high surface-water fertility.

914 In the early Valanginian, high surface-water fertility was suggested in the western
915 Atlantic in DSDP 535 (Gulf of Mexico; Kessels et al., 2006). In the western and northern
916 Altantic (DSDP 534A/603B), Bornemann and Mutterlose (2008) suggested that surface-water
917 productivity was already increasing from the Berriasian-Valanginian boundary prior to the
918 Weissert Event. Whereas, in the Tethys (Vocontian Basin, SE France), generally oligotrophic
919 conditions were recorded in the earliest Valanginian (lowermost NK3 Zone). These
920 oligotrophic conditions were followed by more mesotrophic surface-waters prior to the
921 Weissert Event in the early Valanginian (lower NK3 Zone; Duchamp-Alphonse et al., 2007).
922 In the EAB, and in Hole 416A, the nannofossil production and surface-water fertility were
923 relatively high in the early Valanginian (*N. premolicus* StSz to *N. subtenuis* LSz, lower NK3
924 and lower CC3 subzones).

925 At the early-late Valanginian transition and/or during the incipient Weissert Event,
926 increasing surface-water fertility was observed in several basins. In the Pacific (Site 1149B)
927 and Tethys oceans (Lombardian Basin, northern Italy), higher fertility and primary productivity
928 was demonstrated in the upper NK3 Zone to the NC4A Subzone (Erba et al., 2004; Erba and
929 Tremolada, 2004). In the Vocontian Basin (SE France), increasing calcareous nannofossil
930 fluxes resulted from an increase in surface-water fertility during the Weissert Event, with
931 highest values recorded within the lower NK3B calcareous nannofossil Subzone (upper *B.*

932 *Campylotoxus* to lower *S. verrucosum* ammonite zones; Gréselle et al., 2011; Mattioli et al.,
933 2014). In the western and northern Atlantic (DSDP 534A and 603B), a further increase in
934 surface-water primary productivity was observed during the NK3A Subzone and just prior to
935 the carbon-isotope excursion (Bornemann and Mutterlose, 2008). Also, in the western Atlantic
936 (DSDP 535), Kessels et al. (2006) interpreted higher surface-water fertility in the early late
937 Valanginian. The central Moroccan margin complements these previous records, and similarly
938 demonstrates increasing surface-water fertility and nannofossil production during the Weissert
939 Event on the south Tethyan margin.

940 In the rest of the late Valanginian, during the end or after the Weissert Event, surface-
941 water fertility was observed to globally decrease. In the western Atlantic (DSDP 535), trophic
942 conditions decreased in the late Valanginian (Kessels et al., 2006). In the northern Tethys, a
943 decrease in surface-water fertility was observed in the Lombardian Basin (northern Italy),
944 during the NC4A Subzone when $\delta^{13}C_{carb}$ is decreasing (Erba and Tremolada, 2004). In the
945 Vocontian Basin (SE France), a decrease in both nannofossil fluxes and fertility indicators was
946 observed from the upper part of the Weissert Event (*N. peregrinus* Zone and upper NK3-lower
947 NC4 subzones; Gréselle et al., 2011; Mattioli et al., 2014). Nonetheless, in the Lower Saxony
948 Basin (northern Germany) surface-water fertility increased during the latest Valanginian
949 (Möller et al., 2020). In the EAB, surface-water fertility and nannofossil production decreased
950 at the top of the Weissert Event and after it, as seen in the most complete section of Zalidou.
951 Although, the fertility remained higher than in the early Valanginian. In the Aït Hamouch
952 section, an abrupt increase in surface-water fertility and nannofossil production related to a
953 thick photic zone in an outer shelf setting was observed in the latest Valanginian (upper *C.*
954 *furcillata* StZ, NC4A and upper CC4a subzones).

955 However, in other studied basins, marine surface-water fertility was stable during the
956 Valanginian. In the northern-central Atlantic (DSDP 638, NW Spain), high surface-water

957 fertility was observed throughout the Valanginian (Kessels et al., 2006). Further north in NE
958 Greenland, which was a gateway between the Arctic Ocean and the northern Tethys,
959 oligotrophic conditions were observed during the Valanginian (Pauly et al., 2012). In the eastern
960 Tethys (south and east Carpathians), generally oligotrophic surface-waters were observed
961 during the Berriasian-Valanginian interval, supported by stable nannofossil diversity and
962 abundance (Melinte and Mutterlose, 2001). From the available data, the eastern and
963 northernmost Tethys seem to have been characterized by unchanging paleoceanographic
964 conditions during the Valanginian. This might have been linked to the physiographic
965 characteristics of these basins and the associated atmospheric/oceanic circulation currents (see
966 Price et al., 1995; Poulsen et al., 1998).

967 **5.8 The nannoconid decline**

968 The decrease in the nannoconid abundances is known as the "Nannoconid decline", and
969 is globally recorded to start before the Valanginian positive CIE and spans the Weissert Event
970 (Channell et al., 1993; Bersezio et al., 2002; Erba and Tremolada, 2004; Pauly et al., 2012;
971 Möller et al., 2015). In the western Atlantic, the decrease in the nannoconid abundances was
972 observed from the NK3A to NC4A calcareous nannofossil subzones (DSDP 534A; Bornemann
973 and Mutterlose, 2008). In the Vocontian Basin (SE France), a more complicated decline was
974 observed, such that a first decline was recorded from the NK3A to lower NK3B calcareous
975 nannofossil subzones. This was followed by a brief recovery, then by another decline from the
976 upper NK3B Subzone to NC4 Zone (Barbarin et al., 2012). On the central Moroccan margin,
977 the nannoconid decline similarly started prior to the CI positive-shift. It is generally recorded
978 from the NK3A to lower NK3B subzones (CC3b to lower CC4a subzones). Several authors
979 interpreted the decline to be due to enhanced continental-clastic influx and increased
980 nannofossil primary productivity, and possibly under higher oceanic pCO_2 levels (Erba and
981 Tremolada, 2004; Barbarin et al., 2012; Duchamp-Alphonse et al., 2014). Increasing surface-

water fertility induces the breakdown of the water-column stratification, and then the decrease in the nannoconid population. Various authors proposed that the distribution of narrow-canal *versus* intermediate and wide-canal *Nannoconus* is controlled by fluctuations in nutricline dynamics. In particular, a nutricline rise from the lower to the upper photic zone would lead to the decrease in the narrow-canal forms, these forms are interpreted as deep-dwellers under stratified waters (Erba, 1994, 2004; Duchamp-Alphonse et al., 2014). Since different habitats within the photic zone seem plausible for the big calcifying nannoconids, a deep-dwelling behavior for *N. steinmannii* can be challenged in this study (see section 5.6) confirming the hypothesis of Mattioli et al. (2014). Furthermore, in the Vocontian Basin, high proportions of narrow-canal forms (mainly represented by *N. steinmannii*) correlate with high coccolith abundance (NK3B to lower NC4A calcareous nannofossil subzones; Angles section; Duchamp-Alphonse et al., 2007, 2014). In addition, the highest proportion of narrow-canal nannoconids are recorded within the Weissert Event in the composite section of Vergol/La Charce, when the values of nannofossil fluxes are the highest (Gréselle et al., 2011; Barbarin et al., 2012). On the central Moroccan margin, the nannoconid decline was probably caused by a sea-level fall that gave rise to higher turbidity in the surface-waters. Higher turbidity probably attenuated light penetration, reducing the photic zone and the development of the total nannoconid population. However, enhanced clastic input and associated nutrients led to a shallow nutricline that did not particularly impact *N. steinmannii*.

Moreover, the nannoconid recovery was observed to coincide with the high $\delta^{13}C_{carb}$ values in the Tethys (Vocontian Basin, France) and in the western and northern Atlantic (DSDP 534A and 603B; Erba and Tremolada, 2004; Bornemann and Mutterlose, 2008; Barbarin et al., 2012). This agrees with observations in the EAB, since nannoconids recover during the Weissert Event when the $\delta^{13}C_{carb}$ is high and under conditions of both, high nannofossil

1006 production and surface-water fertility. This suggests that nannoconids do not particularly
1007 disfavor such surface-water conditions.

1008 **6. Conclusions**

1009 The quantitative analyses of calcareous nannofossil assemblages from two onshore
1010 sections belonging to the Essaouira-Agadir Basin (SW Morocco) and one offshore succession
1011 (DSDP Hole 416A, east Atlantic Ocean) allowed to reconstruct the paleoceanographic
1012 conditions on a proximal-distal transect across the Valanginian Weissert Event. This
1013 reconstruction was done in a well-constrained ammonite (for onshore sections only) and
1014 nannofossil biostratigraphic and chemostratigraphic (carbon-isotopes) framework, along with
1015 a detailed sedimentological characterization.

1016 The Weissert Event interval is identified in the onshore sections from the
1017 *Karakaschiceras inostranzewi* to upper *Neocomites peregrinus* Standard Zone (StZ) or from
1018 the upper NK3A to upper NK3B, and upper CC3b to "middle" CC4a calcareous nannofossil
1019 subzones. The Valanginian stage demonstrated variations in surface-water fertility and
1020 nannofossil production. A general paleoceanographic scheme is developed: (1) mesotrophic
1021 and favorable surface-water conditions for the nannofossil community prevailed before the
1022 Weissert Event time interval in the early Valanginian. (2) Surface-water fertility levels
1023 decreased prior to the Weissert Event interval, and a high nannofossil production was
1024 maintained by the eurytopic *Watznaueria barnesiae/fossacincta*. (3) A collapse of the
1025 nannofossil community during the onset of the Weissert Event interval at the early-late
1026 Valanginian transition was caused by a major sea-level fall. (4) A recovery followed in the early
1027 late Valanginian linked to the rising sea-level. (5) The recovery was followed by maximal
1028 nannofossil production associated with high surface-water fertility, recorded in the northern
1029 section during the upper part of the Weissert Event interval in the late Valanginian; or in the
1030 southern section after the Weissert Event interval in the latest Valanginian. Finally, (6) a

decrease in both surface-water fertility and nannofossil production occurred after the Weissert Event interval, although they remained high compared with the early Valanginian. Moreover, the "nannoconid decline" occurred from the early Valanginian to the early late Valanginian. The nannoconid recovery occurred during conditions of high sea-level and high surface-water fertility.

Acknowledgements

This work benefited from financial support by the Ministries of foreign affairs from France and Morocco (PHC project n° 031/STU/13), the French IRD, Campus France, and various grants from the ISTerre laboratory (Grenoble), the Laboratoire de Géologie de Lyon, the OSUG@2020 Labex, the CNRS SYSTER program, and IODP France soutien post-cruise. Additional grants were provided by the French government (bourse BGF), the doctoral school TUE of the Grenoble-Alpes University, and by the TRB team of ISTerre laboratory. We are grateful to the editor Ric Jordan and two anonymous reviewers for both corrections and comments which greatly improved the quality of an earlier version of the manuscript.

7. References:

Aguado, R., Company, M., Castro, J.M., de Gea, G.A., Molina, J.M., Nieto, L.M., Ruiz-Ortiz, P.A., 2018. A new record of the Weissert episode from the Valanginian succession of Cehegín (Subbetic, SE Spain): Bio- and carbon isotope stratigraphy. Cretac. Res. 92, 122–137. https://doi.org/10.1016/j.cretres.2018.07.010

Aguirre-Urreta, M.B., Price, G.D., Ruffell, A.H., Lazo, D.G., Kalin, R.M., Ogle, N., Rawson, P.F., 2008. Southern Hemisphere Early Cretaceous (Valanginian-Early Barremian) carbon and oxygen isotope curves from the Neuquén Basin, Argentina. Cretac. Res. 29, 87–99. https://doi.org/10.1016/j.cretres.2007.04.002

1055 Applegate, J.L., Bergen, J.A., 1988. Cretaceous calcareous nannofossil biostratigraphy of
1056 sediments recovered from the Galicia margin, ODP Leg 103. Proceedings of the Ocean
1057 Drilling Program Leg 103, 293–348.
1058 Aubry, M.-P., Bord, D., Beaufort, L., Kahn, A., Boyd, S., 2005. Trends in size changes in the
1059 coccolithophorids, calcareous nannoplankton, during the Mesozoic: A pilot study.
1060 Micropaleontology 51, 309–318. https://doi.org/10.2113/gsmicropal.51.4.309
1061 Barbarin, N., Bonin, A., Mattioli, E., Pucéat, E., Cappetta, H., Gréselle, B., Pittet, B., Vennin,
1062 E., Joachimski, M., 2012. Evidence for a complex Valanginian nannoconid decline in the
1063 Vocontian basin (South East France). Mar. Micropaleontol. 84–85, 37–53.
1064 https://doi.org/10.1016/j.marmicro.2011.11.005
1065 Bartolini, A., 2003. Cretaceous radiolarian biochronology and carbon isotope stratigraphy of
1066 ODP Site 1149 (northwestern Pacific, Nadezhda Basin). Proceedings of the Ocean Drilling
1067 Program Leg 185, 1-17. https://doi.org/10.2973/odp.proc.sr.185.011.2003
1068 Beaufort, L., Barbarin, N., Gally, Y., 2014. Optical measurements to determine the thickness
1069 of calcite crystals and the mass of thin carbonate particles such as coccoliths. Nat. Protoc.
1070 https://doi.org/10.1038/nprot.2014.028
1071 Bersezio, R., Erba, E., Gorza, M., Riva, A., 2002. Berriasian-Aptian black shales of the
1072 Maiolica formation (Lombardian Basin, Southern Alps, Northern Italy): Local to global
1073 events. Palaeogeogr. Palaeoclimatol. Palaeoecol. 180, 253–275.
1074 https://doi.org/10.1016/S0031-0182(01)00416-3
1075 Bertotti, G., Gouiza, M., 2012. Post-rift vertical movements and horizontal deformations in the
1076 eastern margin of the Central Atlantic: Middle Jurassic to Early Cretaceous evolution of
1077 Morocco. International Journal Earth Sciences (Geologische Rundschau) 101, 2151–2165.

1078 Bordiga, M., Bartol, M., Henderiks, J., 2015. Absolute nannofossil abundance estimates:
1079 Quantifying the pros and cons of different techniques. Rev. Micropaleontol. 58, 155–165.
1080 https://doi.org/10.1016/j.revmic.2015.05.002
1081 Bornemann, A., Mutterlose, J., 2006. Size analyses of the coccolith species *Biscutum constans*
1082 and *Watznaueria barnesiae* from the Late Albian "Niveau Breistroffer" (SE France):
1083 taxonomic and palaeoecological implications 39, 599–615.
1084 https://doi.org/10.1016/j.geobios.2005.05.005
1085 Bornemann, A., Mutterlose, J., 2008. Calcareous nannofossil and $\delta^{13}C$ records from the Early
1086 Cretaceous of the Western Atlantic Ocean: Evidence for enhanced fertilization across the
1087 Berriasian-Valanginian transition. Palaios 23, 821–832.
1088 https://doi.org/10.2110/palo.2007.p07-076r
1089 Bornemann, A., Aschwer, U., Mutterlose, J., 2003. The impact of calcareous nannofossils on
1090 the pelagic carbonate accumulation across the Jurassic-Cretaceous boundary. Palaeogeogr.
1091 Palaeoclimatol. Palaeoecol. 199, 187–228. https://doi.org/10.1016/S0031-
1092 0182(03)00507-8
1093 Bottini, C., Dieni, I., Erba, E., Massari, F., Weissert, H., 2018. The Valanginian Weissert
1094 Oceanic Anoxic Event recorded in Central-Eastern Sardinia (Italy). Riv. Ital. di Paleontol.
1095 e Stratigr. 124 (3), 617–637.
1096 Bown, P.R., 1998. Calcareous nannofossil biostratigraphy. British Micropalaeontological
1097 Society Publications Series. Chapman and Hall; Kluwer Academic.
1098 Bown, P.R., 2005. Early to mid-Cretaceous calcareous nannoplankton from the northwest
1099 Pacific Ocean, Leg 198, Shatsky Rise. Proceedings of the Ocean Drilling Program Leg
1100 198, 1-82. https://doi.org/10.2973/odp.proc.sr.198.103.2005

1101 Bown, P.R., Concheyro, A., 2004. Lower Cretaceous calcareous nannoplankton from the
1102 Neuquén Basin, Argentina. Mar. Micropaleontol. 52, 51–84.
1103 https://doi.org/10.1016/j.marmicro.2004.04.006
1104 Bown, P.R., Lees, J.A., Young, J.R., 2004. Calcareous nannoplankton evolution and diversity
1105 through time. In: Thierstein, H.R., Young, J.R. (Eds.), Coccolithophores: From Molecular
1106 Processes to Global Impact. Springer-Verlag Berlin, Berlin, 481–508.
1107 https://doi.org/10.1007/978-3-662-06278-4_18
1108 Bulot, L.G., Thieuloy, J.-P., 1995. Les biohorizons du Valanginien du Sud-Est de la France :
1109 un outil fondamental pour les corrélations au sein de la Téthys occidentale. Géologie
1110 Alpine. Mémoire Hors Série. 20, 15-41.
1111 Bralower, T.J., 1987. Valanginian to Aptian calcareous nannofossil stratigraphy and correlation
1112 with the upper M-sequence magnetic anomalies. Mar. Micropaleontol. 11, 293–310.
1113 https://doi.org/10.1016/0377-8398(87)90003-X
1114 Bralower, T.J., Monechi, S., Thierstein, H.R., 1989. Calcareous nannofossil zonation of the
1115 Jurassic-Cretaceous boundary interval and correlation with the geomagnetic polarity
1116 timescale. Mar. Micropaleontol. 14, 153–235. https://doi.org/10.1016/0377-
1117 8398(89)90035-2
1118 Bralower, T.J., Leckie, R.M., Sliter, W. V., Thierstein, H.R., 1995. An Integrated Cretaceous
1119 Microfossil Biostratigraphy. Geochronology, Time Scales, Glob. Stratigr. Correl.
1120 https://doi.org/10.2110/pec.95.04.0065
1121 Brenneke, J.C., 1978. A comparison of the stable oxygen and carbon isotope composition of
1122 Early Cretaceous and Late Jurassic carbonates from DSDP Sites 105 and 367. Lancelot,
1123 Y., Siebold, E., et al., Initial Reports of the Deep Sea Drilling Project 41, 937–955.
1124 https://doi.org/10.2973/dsdp.proc.41.135.1978

Čepek, P., Gartner, S., 1980. Mesozoic calcareous nannofossils, Deep Sea Drilling Project Sites 415 and 416, Moroccan Basin 345–351. https://doi.org/10.2973/dsdp.proc.50.108.1980

Channell, J.E.T., Erba, E., Lini, A., 1993. Magnetostratigraphic calibration of the Late Valanginian carbon isotope event in pelagic limestones from Northern Italy and Switzerland. Earth Planet. Sci. Lett. 118, 145–166. https://doi.org/10.1016/0012-821X(93)90165-6

Charbonnier, G., Boulila, S., Gardin, S., Duchamp-Alphonse, S., Adatte, T., Spangenberg, J.E., Föllmi, K.B., Colin, C., Galbrun, B., 2013. Astronomical calibration of the Valanginian "Weissert" episode: The Orpierre marl-limestone succession (Vocontian Basin, southeastern France). Cretac. Res. 45, 25–42. https://doi.org/10.1016/j.cretres.2013.07.003

Charbonnier, G., Duchamp-Alphonse, S., Deconinck, J.F., Adatte, T., Spangenberg, J.E., Colin, C., Föllmi, K.B., 2020. A global palaeoclimatic reconstruction for the Valanginian based on clay mineralogical and geochemical data. Earth-Science Rev. 202, 103092. https://doi.org/10.1016/j.earscirev.2020.103092

Coccioni, R., Erba, E., Premoli-Silva, I., 1992. Barremian-Aptian calcareous plankton biostratigraphy from the Gorgo Cerbara section (Marche, central Italy) and implications for plankton evolution. Cretac. Res. 13, 517–537. https://doi.org/10.1016/0195-6671(92)90015-I

Company, M., Tavera, J.M., 2015. Lower Valanginian ammonite biostratigraphy in the Subbetic Domain (Betic Cordillera, southeastern Spain). Carnets Geol. 15. https://doi.org/10.4267/2042/56745

Cotillon, P., Rio, M., 1984. Cyclic sedimentation in the Cretaceous of Deep Sea Drilling Project Sites 535 and 540 (Gulf of Mexico), 534 (Central Atlantic), and in the Vocontian Basin

(France). Initial Reports of the Deep Sea Drilling Project 77, 339–376. https://doi.org/10.2973/dsdp.proc.77.106.1984

Deres, F., Achéritéguy, J., 1980. Biostratigraphie des Nannoconides. Bulletin des Centres de Recherches Exploration-Production Elf-Aquitaine, 4, 1–53.

Duchamp-Alphonse, S., Gardin, S., Fiet, N., Bartolini, A., Blamart, D., Pagel, M., 2007. Fertilization of the northwestern Tethys (Vocontian basin, SE France) during the Valanginian carbon isotope perturbation: Evidence from calcareous nannofossils and trace element data. Palaeogeogr. Palaeoclimatol. Palaeoecol. 243, 132–151. https://doi.org/10.1016/j.palaeo.2006.07.010

Duchamp-Alphonse, S., Fiet, N., Adatte, T., Pagel, M., 2011. Climate and sea-level variations along the northwestern Tethyan margin during the Valanginian C-isotope excursion: mineralogical evidence from the Vocontian Basin (SE France). Palaeogeography, Palaeoclimatology, Palaeoecology 302, 243-254.

Duchamp-Alphonse, S., Gardin, S., Bartolini, A., 2014. Calcareous nannofossil response to the Weissert episode (Early Cretaceous): Implications for palaeoecological and palaeoceanographic reconstructions. Mar. Micropaleontol. 113, 65–78. https://doi.org/10.1016/j.marmicro.2014.10.002

Dunham, R.J., 1962. Classification of carbonate rocks according to depositional texture. In: Classification of carbonate rocks (W.E. Ham, Ed.), AAPG Memoir 1, 108-121.

Eleson, J.W., Bralower, T.J., 2005. Evidence of changes in surface water temperature and productivity at the Cenomanian/Turonian Boundary. Micropaleontology. 51, 319–332. https://doi.org/10.2113/gsmicropal.51.4.319

Ellouz, N., Patriat, M., Gaulier, J.M., Bouatmani, R., Sabounji, S., 2003. From rifting to Alpine inversion: Mesooic and Cenozoic subsidence history of some Moroccan basins. Sedimentary Geology. 156, 185–212. https://doi.org/10.1016/S0037-0738(02)00288-9

1174 Erba, E., 1992. Middle Cretaceous calcareous nannofossils from the western Pacific (Leg 129):
1175 evidence for paleoequatorial crossings. Proceedings of the Ocean Drilling Program Leg
1176 129, 189–201. https://doi.org/10.2973/odp.proc.sr.129.119.1992
1177 Erba, E., 1994. Nannofossils and superplumes: The early Aptian "nannoconid crisis."
1178 Paleoceanography 9, 483–501.
1179 Erba, E., 2004. Calcareous nannofossils and Mesozoic oceanic anoxic events. Mar.
1180 Micropaleontol. 52, 85–106. https://doi.org/10.1016/j.marmicro.2004.04.007
1181 Erba, E., Quadrio, B., 1987. Biostratigrafia a Nannofossili calcarei Calpionellidi e Foraminiferi
1182 planctonici della Maiolica (Titoniano superiore—Aptiano) nelle Prealpi Bresciane (Italia
1183 Settentrionale). Rivista italiana di paleontologia e stratigrafia. 93 (1), 3-108.
1184 Erba, E., Tremolada, F., 2004. Nannofossil carbonate fluxes during the Early Cretaceous:
1185 Phytoplankton response to nutrification episodes, atmospheric CO_2, and anoxia.
1186 Paleoceanography 19, n/a-n/a. https://doi.org/10.1029/2003PA000884
1187 Erba, E., Castradori, D., Guasti, G., Ripepe, M., 1992. Calcareous nannofossils and
1188 Milankovitch cycles: The example of the Albian Gault Clay Formation (southern
1189 England). Palaeogeogr. Palaeoclimatol. Palaeoecol. 93, 47–69.
1190 Erba, E., Bartolini, A., Larson, R.L., 2004. Valanginian Weissert oceanic anoxic event. Geology
1191 32, 149–152. https://doi.org/10.1130/G20008.1
1192 Ettachfini, El M., 1992. Le Vraconien, Cénomanien et Turonien du Bassin d'Essaouira (Haut
1193 Atlas occidental, Maroc). Ph.D. Thesis, Univ. Paul Sabatier, Toulouse, France, 245p.
1194 https://www.theses.fr/1992TOU30152
1195 Ettachfini M., 2004. Les ammonites néocomiennes dans l'Atlas Atlantique (Maroc):
1196 Biostratigraphie, Paléontologie, Paléobiogéographie et Paléoécologie. Strata, Série 2, Vol.
1197 Mémoires. 43, 1-225

1198 Fernández-Blanco, D., Gouiza, M., Charton, R., Kluge, C., Klaver, J., Brautigam, K., Bertotti,
1199 G., 2020. Anticline growth by shortening during crustal exhumation of the Moroccan
1200 Atlantic margin. Journal of Structural Geology 140, 104125
1201 Ferry, S., Masrour, N., Grosheny, D., 2007. Le Crétacé de la marge atlantique marocaine
1202 (région d'Agadir). Excursion du Groupe Français du Crétacé, Livret-guide, pp. 70.
1203 https://doi.org/https://hal.archives-ouvertes.fr/hal-00686791/document
1204 Föllmi, K.B., 1996. The phosphorus cycle, phosphogenesis and marine phosphate-rich deposits.
1205 Earth-Sci. Rev. 40, 55–124
1206 Föllmi, K.B., Godet, A., Bodin, S., Linder, P., 2006. Interactions between environmental
1207 change and shallow water carbonate buildup along the northern Tethyan margin and their
1208 impact on the Early Cretaceous carbon isotope record. Paleoceanography 21, 1–16.
1209 https://doi.org/10.1029/2006PA001313
1210 Frizon de Lamotte, D., Zizi, M., Missenard, Y., Hafid, M., El Azzouzi, M., Maury, R.C.,
1211 Charrière, A., Taki, Z., Benammi, M., Michard, A., 2008. The Atlas system. Lect. Notes
1212 Earth Sci. 116, 133–202. https://doi.org/10.1007/978-3-540-77076-3_4
1213 Gale, A. S., Mutterlose, J., Batenburg, S., Gradstein, F. M., Agterberg, F. P., Ogg, J. G., &
1214 Petrizzo, M. R., 2020. The Cretaceous Period. In Geologic Time Scale 2020. Elsevier,
1215 1023-1086.
1216 Geisen, M., Bollmann, J., Herrle, J.O., Mutterlose, J., Young, J.R., 1999. Calibration of the
1217 random settling technique for calculation of absolute abundances of calcareous
1218 nannoplankton. Micropaleontology 45, 437–442. https://doi.org/10.2307/1486125
1219 Giraud, F., Olivero, D., Baudin, F., 2003. Minor changes in surface-water fertility across the
1220 oceanic anoxic event 1d (latest Albian, SE France) evidenced by calcareous nannofossils.
1221 Internat. J. Earth Sci 92 (2), 267–284. https://doi.org/10.1007/s00531-003-0319-x

Gómez-Dacal, A.R., Gómez-Peral, L.E., Spalletti, L.A., Sial, A.N., Siccardi, A., Poiré, D.G., 2018. First record of the Valanginian positive carbon isotope anomaly in the Mendoza shelf, Neuquén Basin, Argentina: Palaeoclimatic implications. Andean Geol. 45, 111–129. https://doi.org/10.5027/andgeov45n2-3059

Gréselle, B., Pittet, B., Mattioli, E., Joachimski, M., Barbarin, N., Riquier, L., Reboulet, S., Pucéat, E., 2011. The Valanginian isotope event: A complex suite of palaeoenvironmental perturbations. Palaeogeogr. Palaeoclimatol. Palaeoecol. 306, 41–57. https://doi.org/10.1016/j.palaeo.2011.03.027

Gröcke, D.R., Price, G.D., Robinson, S.A., Baraboshkin, E.Y., Mutterlose, J., Ruffell, A.H., 2005. The Upper Valanginian (Early Cretaceous) positive carbon-isotope event recorded in terrestrial plants. Earth Planet. Sci. Lett. 240, 495–509. https://doi.org/10.1016/j.epsl.2005.09.001

Grün, W. & Allemann, F. (1975). The Lower Cretaceous of Caravaca (Spain): Berriasian calcareous nannoplankton of the Miravetes Section (Subbetic Zone, Prov. of Murcia). Eclogae Geologicae Helvetiae. 68, 147-211. http://dx.doi.org/10.5169/seals-164382.

Hammer, Ø., Harper, D.A.T., Ryan, P.D., 2001. PAST: Paleontological Statistics Software Package for Education and Data Analysis. Palaeontologia Electronica 4 (1), pp. 9.

Haq, B.U., 2014. Cretaceous eustasy revisited. Glob. Planet. Change 113, 44–58. https://doi.org/10.1016/j.gloplacha.2013.12.007

Hay, W.W., DeConto, R.M., Wold, C.N., Wilson, K.M., Voigt, S., Schulz, M., Wold, A.R., Dullo, W.C., Ronov, A.B., Balukhovsky, A.N., Söding, E., 1999. Alternative global Cretaceous paleogeography. Spec. Pap. Geol. Soc. Am., pp. 332. https://doi.org/10.1130/0-8137-2332-9.1

1245 Hennig, S., Weissert, H., Bulot, L., 1999. C-isotope stratigraphy, a calibration tool between
1246 ammonite- and magnetostratigraphy: The Valanginian-Hauterivian transition. Geol.
1247 Carpathica 50, 91–96.
1248 Herrle, J.O., 2002. Reconstructing nutricline dynamics of mid-Cretaceous oceans: Evidence
1249 from calcareous nannofossils from the Niveau Paquier black shale (SE France). Mar.
1250 Micropaleontol. 47, 307–321. https://doi.org/10.1016/S0377-8398(02)00133-0
1251 Herrle, J.O., Pross, J., Friedrich, O., Hemleben, C., 2003. Short-term environmental changes in
1252 the Cretaceous Tethyan Ocean: micropalaeontological evidence from the Early Albian
1253 Oceanic Anoxic Event 1b. Terra Nova. 15 (1), 14-19. https://doi.org/10.1046/j.1365-
1254 3121.2003.00448.x
1255 Immenhauser, A., Holmden, C., Patterson, W.P., 2008. Interpreting the carbon-isotope record
1256 of ancient shallow epeiric seas: Lessons from the recent, in: Special Paper - Geological
1257 Association of Canada., 137–174.
1258 Jaillard, E., Chihaoui, A., Latil, J.-L., Zghal, I., 2021. Sequences, discontinuities and water
1259 stratification in a low-energy ramp: the Early Albian sedimentation in central Tunisia.
1260 Internat. J. Earth Sci. 110, 263-285.
1261 Kender, S., Kaminski, M.A., 2017. Modern deep-water agglutinated foraminifera from IODP
1262 Expedition 323, Bering Sea: ecological and taxonomic implications. Journal of
1263 Micropalaeontology 36, 195–218.
1264 Kenjo, S., Reboulet, S., Mattioli, E., Ma'louleh, K., 2021. The Berriasian–Valanginian
1265 boundary in the Mediterranean Province of the Tethyan Realm: Ammonite and calcareous
1266 nannofossil biostratigraphy of the Vergol section (Montbrun-les-Bains, SE France),
1267 candidate for the Valanginian GSSP. Cretac. Res. 121, 104738.
1268 https://doi.org/10.1016/j.cretres.2020.104738

1269 Kessels, K., Mutterlose, J., Michalzik, D., 2006. Early Cretaceous (Valanginian - Hauterivian)
1270 calcareous nannofossils and isotopes of the northern hemisphere: Proxies for the
1271 understanding of Cretaceous climate. Lethaia 39, 157–172.
1272 https://doi.org/10.1080/00241160600763925
1273 Kuhnt, W., Moullade, M., Kaminski, M.A., 1996. Ecological structuring and evolution of deep-
1274 sea agglutinated foraminifera - A review. Revue de Micropaléontologie 39, 271–281.
1275 Kujau, A., Heimhofer, U., Ostertag-Henning, C., Gréselle, B., Mutterlose, J., 2012. No evidence
1276 for anoxia during the Valanginian carbon isotope event - An organic-geochemical study
1277 from the Vocontian Basin, SE France. Glob. Planet. Change 92, 92–104.
1278 https://doi.org/10.1016/j.gloplacha.2012.04.007
1279 Kujau, A., Heimhofer, U., Hochuli, P.A., Pauly, S., Morales, C., Adatte, T., Föllmi, K., Ploch,
1280 I., Mutterlose, J., 2013. Reconstructing Valanginian (Early Cretaceous) mid-latitude
1281 vegetation and climate dynamics based on spore-pollen assemblages. Rev. Palaeobot.
1282 Palynol. 197, 50–69. https://doi.org/10.1016/j.revpalbo.2013.05.003
1283 Lancelot, Y., Winterer, E.L., Bosellini, A., Boutefeu, G.A., Boyce, R.E., Cepek, P., Fritz, D.,
1284 Galimov, E.M., Melguen, M., Price, I., Schlager, W., Sliter, W., Taguchi, K., Vincent, E.,
1285 Westberg, J., 1980. Site 416, in the Moroccan Basin, Deep Sea Drilling Project Leg 50.
1286 Initial Reports of the Deep Sea Drilling Project 50, 115–301.
1287 https://doi.org/10.2973/dsdp.proc.50.104.1980
1288 Lees, J.A., 2002. Calcareous nannofossil biogeography illustrates palaeoclimate change in the
1289 Late Cretaceous Indian Ocean. Cretac. Res. 23 (5), 537-634.
1290 https://doi.org/10.1006/cres.2003.1021
1291 Lees, J.A., Bown, P.R., Mattioli, E., 2005. Problems with proxies? Cautionary tales of
1292 calcareous nannofossil paleoenvironmental indicators. Micropaleontology 51, 333–343.
1293 https://doi.org/10.2113/gsmicropal.51.4.333

1294 Lini, A., Weissert, H., Erba, E., 1992. The Valanginian carbon isotope event: a first episode of
1295 greenhouse climate conditions during the Cretaceous. Terra Nova 4, 374–384.
1296 https://doi.org/10.1111/j.1365-3121.1992.tb00826.x
1297 Lozar, F., Tremolada, F., 2003. Calcareous nannofossil biostratigraphy of Cretaceous sediments
1298 recovered at ODP Site 1149 (Leg 185, Nadezhda Basin, western Pacific). Proceedings of
1299 the Ocean Drilling Program Leg 185, 1–21.
1300 https://doi.org/10.2973/odp.proc.sr.185.010.2003
1301 Lupi, C., Bordiga, M., Sacchi, R., Galinetto, P., Beaufort, L., Cobianchi, M., 2016. Do sample
1302 preparation techniques affect the relative abundance of *Florisphaera profunda*? Mar.
1303 Micropaleontol. 127, 42–49. https://doi.org/10.1016/j.marmicro.2016.07.007
1304 Martinez, M., Deconinck, J.F., Pellenard, P., Reboulet, S., Riquier, L., 2013. Astrochronology
1305 of the Valanginian Stage from reference sections (Vocontian Basin, France) and
1306 palaeoenvironmental implications for the Weissert Event. Palaeogeogr. Palaeoclimatol.
1307 Palaeoecol. 376, 91–102. https://doi.org/10.1016/j.palaeo.2013.02.021
1308 Martinez, M., Deconinck, J.F., Pellenard, P., Riquier, L., Company, M., Reboulet, S., Moiroud,
1309 M., 2015. Astrochronology of the Valanginian-Hauterivian stages (Early Cretaceous):
1310 Chronological relationships between the Paraná-Etendeka large igneous province and the
1311 Weissert and the Faraoni events. Glob. Planet. Change 131, 158–173.
1312 https://doi.org/10.1016/j.gloplacha.2015.06.001
1313 Mattioli, E., Pittet, B., Riquier, L., Grossi, V., 2014. The mid-Valanginian Weissert Event as
1314 recorded by calcareous nannoplankton in the Vocontian Basin. Palaeogeogr.
1315 Palaeoclimatol. Palaeoecol. 414, 472–485. https://doi.org/10.1016/j.palaeo.2014.09.030
1316 McArthur, J.M., Janssen, N.M.M., Reboulet, S., Leng, M.J., Thirlwall, M.F., van de
1317 Schootbrugge, B., 2007. Palaeotemperatures, polar ice-volume, and isotope stratigraphy
1318 (Mg/Ca, $\delta^{18}O$, $\delta^{13}C$, $^{87}Sr/^{86}Sr$): The Early Cretaceous (Berriasian, Valanginian,

1319 Hauterivian). Palaeogeogr. Palaeoclimatol. Palaeoecol. 248, 391–430.
1320 https://doi.org/10.1016/j.palaeo.2006.12.015
1321 Meissner, P., Mutterlose, J., Bodin, S., 2015. Latitudinal temperature trends in the northern
1322 hemisphere during the Early Cretaceous (Valanginian-Hauterivian). Palaeogeogr.
1323 Palaeoclimatol. Palaeoecol. 424, 17–39. https://doi.org/10.1016/j.palaeo.2015.02.003
1324 Melinte, M., Mutterlose, J., 2001. A Valanginian (Early Cretaceous) "boreal nannoplankton
1325 excursion" in sections from Romania. Mar. Micropaleontol. 43, 1–25.
1326 https://doi.org/10.1016/S0377-8398(01)00022-6
1327 Menini, A., Mattioli, E., Spangenberg, J.E., Pittet, B., Suan, G., 2019. New calcareous
1328 nannofossil and carbon isotope data for the Pliensbachian/Toarcian boundary (Early
1329 Jurassic) in the western Tethys and their paleoenvironmental implications. Newsletters
1330 Stratigr. 52, 173–196. https://doi.org/10.1127/nos/2018/0476
1331 Michel, J., Borgomano, J., Reijmer, J.J.G., 2018. Heterozoan carbonates: When, where and
1332 why? A synthesis on parameters controlling carbonate production and occurrences. Earth-
1333 Science Reviews 182, 50–67.
1334 Möller, C., Mutterlose, J., Alsen, P., 2015. Integrated stratigraphy of Lower Cretaceous
1335 sediments (Ryazanian–Hauterivian) from North-East Greenland. Palaeogeography,
1336 Palaeoclimatology, Palaeoecology 437, 85-97.
1337 https://doi.org/10.1016/j.palaeo.2015.07.014
1338 Möller, C., Bornemann, A., Mutterlose, J., 2020. Climate and paleoceanography controlled size
1339 variations of calcareous nannofossils during the Valanginian Weissert Event (Early
1340 Cretaceous). Marine Micropaleontology, 157, 101875.
1341 https://doi.org/10.1016/j.marmicro.2020.101875
1342 Morales, C., Kujau, A., Heimhofer, U., Mutterlose, J., Spangenberg, J.E., Adatte, T., Ploch, I.,
1343 Föllmi, K.B., 2015. Palaeoclimate and palaeoenvironmental changes through the onset of

1344 the Valanginian carbon-isotope excursion: Evidence from the Polish Basin. Palaeogeogr.
1345 Palaeoclimatol. Palaeoecol. 426, 183–198. https://doi.org/10.1016/j.palaeo.2015.03.013
1346 Müller, G., Gastner, M., 1971. The "Karbonat-Bombe", a simple device for the determination
1347 of carbonate content in sediment, soils, and other materials. Neues Jahrbuch für
1348 Mineralogie-Monatshefte 10, 466-469.
1349 Mutterlose, J., 1992a. Lower Cretaceous nannofossil biostratigraphy off northwestern Australia
1350 (Leg 123). Proceedings of the Ocean Drilling Program Leg 123, 343-368.
1351 Mutterlose, J., 1992b. Migration and evolution patterns of floras and faunas in marine Early
1352 Cretaceous sediments of NW Europe. Palaeogeogr. Palaeoclimatol. Palaeoecol. 94, 261–
1353 282. https://doi.org/10.1016/0031-0182(92)90123-M
1354 Mutterlose, J., Kessels, K., 2000. Early Cretaceous calcareous nannofossils from high latitudes:
1355 Implications for palaeobiogeography and palaeoclimate. Palaeogeogr. Palaeoclimatol.
1356 Palaeoecol. 160, 347–372. https://doi.org/10.1016/S0031-0182(00)00082-1
1357 Mutterlose, J., Brumsack, H., Flögel, S., Hay, W., Klein, C., Langrock, U., Lipinski, M.,
1358 Ricken, W., Söding, E., Stein, R., Swientek, O., 2003. The Greenland-Norwegian Seaway:
1359 A key area for understanding Late Jurassic to Early Cretaceous paleoenvironments.
1360 Paleoceanography 18 (1). https://doi.org/10.1029/2001PA000625
1361 Mutterlose, J., Bornemann, A., Herrle, J., 2005. Mesozoic calcareous nannofossils - state of the
1362 art. Paläontologische Zeitschrift 79, 113–133.
1363 Mutterlose, J., Rawson, P.F., Reboulet, S., Baudin, F., Bulot, L., Emmanuel, L., Gardin, S.,
1364 Martinez, M., Renard, M., 2020. The Global Boundary Stratotype Section and Point
1365 (GSSP) for the base of the Hauterivian Stage (Lower Cretaceous), La Charce, southeast
1366 France. Episodes Journal of International Geoscience.
1367 https://doi.org/10.18814/epiiugs/2020/020072

1368 Nunn, E. V., Price, G.D., Gröcke, D.R., Baraboshkin, E.Y., Leng, M.J., Hart, M.B., 2010. The
1369 Valanginian positive carbon isotope event in Arctic Russia: Evidence from terrestrial and
1370 marine isotope records and implications for global carbon cycling. Cretac. Res. 31, 577–
1371 592. https://doi.org/10.1016/j.cretres.2010.07.007
1372 Ouajhain, B., Daoudi, L., Medina, F., Rocha, F., 2009. Contrôle paléogéographique de la
1373 sédimentation argileuse du Jurassique du bassin atlasique d'Essaouira (haut atlas
1374 occidental, Maroc). Comun. Geol. 96, 51–66.
1375 Pauly, S., Mutterlose, J., Alsen, P., 2012. Early Cretaceous palaeoceanography of the
1376 Greenland-Norwegian Seaway evidenced by calcareous nannofossils. Mar.
1377 Micropaleontol. 90 (91), 72–85. https://doi.org/10.1016/j.marmicro.2012.04.004
1378 Perch-Nielsen, K., 1979. Calcareous nannofossils from the Cretaceous between the North Sea
1379 and the Mediterranean. Aspekte der Kreide Europas, IUGS Series A. 6, 223-272.
1380 Perch-Nielsen, K., 1985. Mesozoic Calcareous nannofossils. In Bolli, H.M., Saunders, J.B. and
1381 Perch-Nielsen, K., Eds., Plankton Stratigraphy, Cambridge Universitry Press, Cambridge,
1382 329-426.
1383 Peybernes, C., Giraud, F., Jaillard, E., Robert, E., Masrour, M., Aoutem, M., Içame, N., 2013.
1384 Stratigraphic framework and calcareous nannofossil productivity of the Essaouira-Agadir
1385 Basin (Morocco) during the Aptian-Early Albian: Comparison with the north-Tethyan
1386 margin. Cretac. Res. 39, 149–169. https://doi.org/10.1016/j.cretres.2012.02.017
1387 Pittet, B., Mattioli, E., 2002. The carbonate signal and calcareous nannofossil distribution in an
1388 Upper Jurassic section (Balingen-Tieringen, Late Oxfordian, southern Germany).
1389 Palaeogeogr. Palaeoclimatol. Palaeoecol. 179, 71–96. https://doi.org/10.1016/S0031-
1390 0182(01)00409-6
1391 Pohl, A., Laugié, M., Borgomano, J., Michel, J., Lanteaume, C., Scotese, C.R., Frau, C., Poli,
1392 E., Donnadieu, Y., 2019. Quantifying the paleogeographic driver of Cretaceous carbonate

platform development using paleoecological niche modeling. Palaeogeogr. Palaeoclim. Palaeoecol. 514, 222–232. https://doi.org/10.1016/j.palaeo.2018.10.017

Poulsen, C.J., Seidov, D., Barron, E.J., Peterson, W.H., 1998. The impact of paleogeographic evolution on the surface oceanic circulation and the marine environment within the mid-Cretaceous Tethys. Paleoceanography 13, 546–559. https://doi.org/10.1029/98PA01789

Premoli Silvá, I., Erba, E., Emilia Tornaghi, M., 1989. Paleoenvironmental signals and changes in surface fertility in mid Cretaceous C_{org}-rich pelagic facies of the Fucoid Marls (Central Italy). Geobios 22, 225–236. https://doi.org/10.1016/S0016-6995(89)80059-2

Price, G.D., Sellwood, B.W., Valdes, P.J., 1995. Sedimentological evaluation of general circulation model simulations for the "greenhouse" Earth: Cretaceous and Jurassic case studies. Sediment. Geol. 100, 159–180. https://doi.org/10.1016/0037-0738(95)00106-9

Price, G.D., Mutterlose, J., 2004. Isotopic signals from late Jurassic-early Cretaceous (Volgian-Valanginian) sub-Arctic belemnites, Yatria River, Western Siberia. J. Geol. Soc. London. 161, 959–968. https://doi.org/10.1144/0016-764903-169

Puhfal, P.K., Groat, L.A., 2017. Sedimentary and igneous phosphate deposits: formation and exploration. Econ. Geol. 112, 483–516.

Reboulet, S., 1996. L'évolution des ammonites du Valanginien-Hauterivien inférieur du bassin vocontien et de la plate-forme provençale (S-E de la France): relations avec la stratigraphie séquentielle et implications biostratigraphiques. Travaux et Documents des Laboratoires de Géologie de Lyon 137 (1), 3-371.

Reboulet, S., Atrops, F., 1999. Comments and proposals about the Valanginian-Lower Hauterivian ammonite zonation of south-eastern France. Eclogae Geol. Helv. 92 (2), 183-198.

Reboulet, S., Mattioli, E., Pittet, B., Baudin, F., Olivero, D., Proux, O., 2003. Ammonoid and nannoplankton abundance in Valanginian (early Cretaceous) limestone–marl successions

1418 from the southeast France Basin: carbonate dilution or productivity? Palaeogeography,
1419 Palaeoclimatology, Palaeoecology 201, 113-139.
1420 Reboulet, S., Szives, O., Aguirre-Urreta, B., Barragán, R., Company, M., Frau, C., Kakabadze,
1421 M. V., Klein, J., Moreno-Bedmar, J.A., Lukeneder, A., Pictet, A., Ploch, I., Raisossadat,
1422 S.N., Vašíček, Z., Baraboshkin, E.J., Mitta, V. V., 2018. Report on the 6th International
1423 Meeting of the IUGS Lower Cretaceous Ammonite Working Group, the Kilian Group
1424 (Vienna, Austria, 20th August 2017). Cretac. Res. 91, 100–110.
1425 https://doi.org/10.1016/j.cretres.2018.05.008
1426 Reolid, M., Nagy, J., Rodríguez-Tovar, F.J., Olóriz, F., 2008. Foraminiferal assemblages as
1427 palaeoenvironmental bioindicators in Late Jurassic epicontinental Platforms: Relation
1428 with trophic conditions. Acta Palaeontologica Polonica 53, 705–722.
1429 Roth, P.H., 1978. Cretaceous nannoplankton biostratigraphy and oceanography of the
1430 northwestern Atlantic Ocean. Initial Reports of the Deep Sea Drilling Project 44, 731–759.
1431 https://doi.org/10.2973/dsdp.proc.44.134.1978
1432 Roth, P. H., 1981. Mid-Cretaceous calcareous nannoplankton from Central Pacific: implication
1433 for paleoceanography. Initial Reports of the Deep Sea Drilling Project 75, 651–655.
1434 Roth, P.H., 1983. Jurassic and Lower Cretaceous calcareous nannofossils in the western North
1435 Atlantic (Site 534): biostratigraphy, preservation, and some observations on biogeography
1436 and paleoceanography. Initial Reports of the Deep Sea Drilling Project 76, 587–621.
1437 https://doi.org/10.2973/dsdp.proc.76.125.1983
1438 Roth, P.H., 1989. Ocean circulation and calcareous nannoplankton evolution during the Jurassic
1439 and Cretaceous. Palaeogeog., Palaeoclimat., Palaeoec. 74 (1-2), 111-26.
1440 https://doi.org/10.1016/0031-0182(89)90022-9

1441 Roth, P.H., Thierstein, H., 1972. Calcareous nannoplankton: Leg 14 of the Deep Sea Drilling
1442 Program. Initial Reports of the Deep Sea Drilling Project 14, 421–486.
1443 https://doi.org/10.2973/dsdp.proc.14.114.1972
1444 Roth, P. H., Bowdler, J.L., 1981. Middle Cretaceous calcareous nannoplankton biogeography
1445 and oceanography of the Atlantic Ocean. Soc. Econ. Paleontol. Miner. Spec. Publ. 32,
1446 517–546.
1447 Roth, P.H., Krumbach, K.R., 1986. Middle Cretaceous calcareous nannofossil biogeography
1448 and preservation in the Atlantic and Indian oceans: Implications for paleoceanography.
1449 Mar. Micropaleontol. 10, 235–266. https://doi.org/10.1016/0377-8398(86)90031-9
1450 Sahabi, M., Aslanian, D., Olivet, J.L., 2004. Un nouveau point de départ pour l'histoire de
1451 l'Atlantique central. Comptes Rendus - Geosci. 336, 1041–1052.
1452 https://doi.org/10.1016/j.crte.2004.03.017
1453 Schlager, W., 1980. Mesozoic Calciturbidites in Deep Sea Drilling Project Hole 416A
1454 Recognition of a Drowned Carbonate Platform. Initial Reports of the Deep Sea Drilling
1455 Project 50, 733–749. https://doi.org/10.2973/dsdp.proc.50.138.1980
1456 Shmeit, M., 2021. Apports continentaux versus upwellings dans le déclenchement de
1457 l'événement océanique anoxique Weissert (~ 137 Ma): contraintes micropaléontologiques
1458 et isotopiques. Ph.D. Thesis, Univ. Grenoble Alpes, France, 304p.
1459 Sissingh, W., 1977. Biostratigraphy of Cretaceous calcareous nannoplankton. Geologie en
1460 Mijnbouw 56, 37–65.
1461 Sliter, W. V., 1980. Mesozoic foraminifers and deep-sea benthic environments from Deep Sea
1462 Drilling Project sites 415 and 416, eastern North Atlantic. Initial Reports of the Deep Sea
1463 Drilling Project 50, 353–427. https://doi.org/10.2973/dsdp.proc.50.109.1980

1464 Sprovieri, M., Coccioni, R., Lirer, F., Pelosi, N., Lozar, F., 2006. Orbital tuning of a lower
1465 Cretaceous composite record (Maiolica Formation, central Italy). Paleoceanography 21
1466 (4). https://doi.org/10.1029/2005PA001224
1467 Stets, J., Wurster, P., 1982. Atlas and Atlantic - structural relations. Geol. northwest African
1468 Cont. margin 69–85. https://doi.org/10.1007/978-3-642-68409-8_5
1469 Street, C., Bown, P.R., 2000. Palaeobiogeography of Early Cretaceous (Berriasian-Barremian)
1470 calcareous nannoplankton. Mar. Micropaleontol. 39, 265–291.
1471 https://doi.org/10.1016/S0377-8398(00)00024-4
1472 Suchéras-Marx, B., Escarguel, G., Ferreira, J., Hammer, Ø., 2019. Statistical confidence
1473 intervals for relative abundances and abundance-based ratios: Simple practical solutions
1474 for an old overlooked question. Mar. Micropaleontol. 151, 101751.
1475 https://doi.org/10.1016/j.marmicro.2019.101751
1476 Tari, G., Jabour, H., 2013. Salt tectonics along the Atlantic margin of Morocco. Geological
1477 Society, London, Special Publications 369, 337-353.
1478 Thierstein, H.R., 1980. Selective dissolution of Late Cretaceous and Earliest Tertiary calcareous
1479 nannofossils: Experimental evidence. Cret. Res. 1 (2), 165-176.
1480 https://doi.org/10.1016/0195-6671(80)90023-3
1481 Trabucho Alexandre, J., Van Gilst, R.I., Rodríguez-López, J.P., De Boer, P.L., 2011. The
1482 sedimentary expression of oceanic anoxic event 1b in the North Atlantic. Sedimentology
1483 58 (5), 1217–1246. https://doi.org/10.1111/j.1365-3091.2010.01202.x
1484 Tremolada, F., Erba, E., Bralower, T.J., 2006. Late Barremian to early Aptian calcareous
1485 nannofossil paleoceanography and paleoecology from the Ocean Drilling Program Hole
1486 641C (Galicia Margin). Cretac. Res. 27, 887–897.
1487 https://doi.org/10.1016/j.cretres.2006.04.007

1488 Watkins, D.K., 1989. Nannoplankton productivity fluctuations and rhythmically-bedded
1489 pelagic carbonates of the greenhorn limestone (upper Cretaceous). Palaeogeogr.
1490 Palaeoclimatol. Palaeoecol. 74, 75–86. https://doi.org/10.1016/0031-0182(89)90020-5
1491 Weissert, H., Lini, A., Föllmi, K.B., Kuhn, O., 1998. Correlation of Early Cretaceous carbon
1492 isotope stratigraphy and platform drowning events: A possible link? Palaeogeogr.
1493 Palaeoclimatol. Palaeoecol. 137, 189–203. https://doi.org/10.1016/S0031-
1494 0182(97)00109-0
1495 Weissert, H., Erba, E., 2004. Volcanism, CO_2 and palaeoclimate: a Late Jurassic-Early
1496 Cretaceous carbon and oxygen isotope record. J. Geol. Soc. London. 161, 695–702.
1497 https://doi.org/10.1144/0016-764903-087
1498 Williams, J.R., Bralower, T.J., 1995. Nannofossil assemblages, fine fraction stable isotopes,
1499 and the paleoceanography of the Valanginian-Barremian (Early Cretaceous) North Sea
1500 Basin. Paleoceanography 10, 815–839. https://doi.org/10.1029/95PA00977
1501 Wippich, M.G.E., 2001. Die tiefe Unter-Kreide (Berrias bis Unter-Hauterive) im
1502 südwestmarokkanischen Becken: Ammonitenfauna, Bio-und Sequenzstratigraphie. PhD
1503 thesis, Bochum University/Universitat Bochu, pp. 142.
1504 Wippich, M.G.E., 2003. Valanginian (Early Cretaceous) ammonite faunas from the western
1505 High Atlas, Morocco, and the recognition of western Mediterranean “standard” zones.
1506 Cretac. Res. 24, 357–374. https://doi.org/10.1016/S0195-6671(03)00049-1
1507 Wortmann, U.G., Weissert, H., 2000. Tying platform drowning to perturbations of the global
1508 carbon cycle with a delta $\delta^{13}C_{Org}$-curve from the Valanginian of DSDP Site 416. Terra
1509 Nova 12, 289–294. https://doi.org/10.1046/j.1365-3121.2000.00312.x
1510 Young, J.R., Bown P.R., Lees J.A., 2017. Nannotax3 website. International Nannoplankton
1511 Association. Accessed 10 April 2022. URL: http://www.mikrotax.org/Nannotax3